General Disclaimer

One or more of the Following Statements may affect this Document

- This document has been reproduced from the best copy furnished by the organizational source. It is being released in the interest of making available as much information as possible.

- This document may contain data, which exceeds the sheet parameters. It was furnished in this condition by the organizational source and is the best copy available.

- This document may contain tone-on-tone or color graphs, charts and/or pictures, which have been reproduced in black and white.

- This document is paginated as submitted by the original source.

- Portions of this document are not fully legible due to the historical nature of some of the material. However, it is the best reproduction available from the original submission.

NASA TECHNICAL MEMORANDUM

NASA TM X-62,488

NASA TM X-62,488

EVALUATION OF MEAN AND TURBULENT VELOCITY MEASUREMENTS IN SUBSONIC ACCELERATED BOUNDARY LAYERS

V. A. Sandborn
Colorado State University
Fort Collins, CO 80523

and

H. L. Seegmiller
Ames Research Center
Moffett Field, CA 94035

March 1976

1. Report No.	2. Government Accession No.	3. Recipient's Catalog No.
NASA TM X-62,488		

4. Title and Subtitle	5. Report Date
EVALUATION OF MEAN AND TURBULENT VELOCITY MEASUREMENTS IN SUBSONIC ACCELERATED BOUNDARY LAYERS	6. Performing Organization Code

7. Author(s)	8. Performing Organization Report No.
V. A. Sandborn* and H. L. Seegmiller	A-6278
	10. Work Unit No. 505-06-13-01-00-21
9. Performing Organization Name and Address Ames Research Center, Moffett Field, CA 94035 *Colorado State University, Fort Collins, CO 80523	11. Contract or Grant No.
	13. Type of Report and Period Covered Technical Memorandum
12. Sponsoring Agency Name and Address National Aeronautics and Space Administration Washington, D. C. 20546	14. Sponsoring Agency Code

15. Supplementary Notes

16. Abstract

Exploratory measurements of the mean and turbulent flow in the wall boundary layer of a 15.5- by 10.2-cm channel were obtained as part of an instrumentation development program for measurements in compressible flow. Mean surface and flow-field surveys were obtained at channel Mach numbers ranging from 0.2 to 0.9. The mean velocity distributions were obtained with total pressure probes and a laser velocimeter. At a channel Mach number of 0.2, several types of hot-wire probes were used to obtain both velocity fluctuations and Reynolds shear-stress results.

17. Key Words (Suggested by Author(s))	18. Distribution Statement
Turbulent boundary layer Hot-wire anemometry Subsonic flow	Unlimited STAR Category – 34

19. Security Classif. (of this report)	20. Security Classif. (of this page)	21. No. of Pages	22. Price*
Unclassified	Unclassified	43	$3.75

*For sale by the National Technical Information Service, Springfield, Virginia 22151

NOTATION

A	King's law calibration constant
B	King's law calibration constant
c_f	skin-friction coefficient
D	diameter
E	voltage drop across hot wire and hot film
F	compressible skin-friction correction
H	boundary-layer form factor
ℓ	wire length
M	Mach number
p	pressure
R	Reynolds number
S	hot-wire and hot-film sensitivity and overheat coefficients
T	temperature
U	longitudinal mean velocity
U_τ	shear stress velocity
u	longitudinal turbulent velocity
V	vertical mean velocity
v	vertical turbulent velocity
x, y	orthogonal Cartesian coordinates
α	thermal coefficient of resistance
δ	boundary-layer thickness
δ^*	boundary-layer displacement thickness
θ	boundary-layer momentum thickness

μ coefficient of viscosity

ν kinematic viscosity

ρ mean density

ρ' turbulent density fluctuations

τ shear stress

ϕ yaw angle

$\langle\langle\ \rangle\rangle$ root mean square

Subscripts

a ambient air temperature

c compressible

e boundary-layer edge

n normal or vertical hot wire

o inlet or stagnation conditions

s static conditions

u longitudinal velocity sensitivity

v vertical velocity sensitivity

w wall conditions

y yawed wire

θ based on momentum thickness

∞ free stream

1 film number 1

2 film number 2

Superscript

$(\bar{\ })$ time average

EVALUATION OF MEAN AND TURBULENT VELOCITY MEASUREMENTS IN SUBSONIC ACCELERATED BOUNDARY LAYERS

V. A. Sandborn* and H. L. Seegmiller

Ames Research Center

SUMMARY

Exploratory measurements of the mean and turbulent flow in the wall boundary layer of a 15.5- by 10.2-cm channel were obtained as part of an instrumentation development program for measurements in compressible flow. Mean surface and flow-field surveys were obtained at channel Mach numbers ranging from 0.2 to 0.9. The mean velocity distributions were obtained with total pressure probes and a laser velocimeter. At a channel Mach number of 0.2, several types of hot-wire probes were used to obtain both velocity fluctuations and Reynolds shear-stress results.

INTRODUCTION

Only a limited amount of mean and fluctuating data have been reported for turbulent boundary layers in subsonic, compressible flow (ref. 1), chiefly because of the difficulties involved with obtaining these measurements; for example, probe interference effects and probe breakage problems caused by the high dynamic pressures. Additionally, no reliable technique has been developed to directly measure the turbulent shear stress near the wall in compressible flows (ref. 1).

In this report, we first present a thorough documentation of the mean-surface and flow-field quantities in a subsonic, variable Mach-number channel for Mach numbers of 0.2 to 0.9. The mean flow-field measurements were obtained with conventional pitot probes and checked with a laser velocimeter to insure that the data were free from probe-interference effects. The principal purpose of the mean-flow documentation was to provide high-quality data which could be used for evaluating direct measurements of the turbulent shear stress.

Secondly, we present an evaluation of hot-wire and split-film probes with respect to their use in the measuring of turbulent intensities and shear stress in a subsonic boundary layer. To date, the split-film probe has only been employed in water flow and in air at extremely low velocities. This probe offers the advantage of being an order of magnitude smaller in the vertical direction than the X-wire probe. In particular, a detailed investigation was conducted to isolate the source of the problems encountered in the measurement of turbulent shear stress near the wall. To avoid the additional problems of compressibility, the fluctuating measurements in the boundary layer were limited to a Mach number of 0.22.

---

*Colorado State University, Fort Collins, CO 80523.

TEST FACILITY AND INSTRUMENTATION

Facility

The study was conducted in a 15.2- by 10.2-cm channel, shown schematically in figure 1. Figure 2 is a photograph of the test section and the laser beams. The channel had an atmospheric inlet and a vacuum valve to a steam-driven exhauster which drew the air through the test section. Flow was controlled by restricting the exit opening with flexible metal plates which choked the flow downstream of the test section. Because of the atmospheric inlet, it was not possible to independently control the flow Mach number and Reynolds number. Filter paper was used at the inlet to control the dust particles and reduce the incidence of hot-wire breakage. The filter paper provides approximately 1 hr of essentially particle-free flow at the higher mass flow rates, and a great deal longer time at the lower velocities. For Mach numbers above about 0.65, condensed water vapor was present in the flow through the test section. Mean-flow surveys were obtained at 28.6 (window station), 20.4, and 0.0 cm downstream from static-pressure tap 1. The fluctuating surveys were obtained at the window station.

Instrumentation

Static-pressure orifices– The channel was equipped with five wall-static-pressure taps, each with a 0.051-cm diam (see fig. 1). A quartz bourdon tube, absolute-pressure transducer was used for the static-pressure measurements.

Surface-skin friction– The skin friction was measured directly with a floating-element balance at the window station. Direct calibrations, using weights hung from the sensing element, were performed before and after the test series; they were repeatable to within 5 percent. Corrections for bouyancy effects caused by the axial pressure gradient were negligible.

A preliminary attempt was made to evaluate the difference in static-pressure readings between a 0.051- and a 0.102-cm-diam static hole as a measure of the local wall shear stress. The fluctuations in the static-pressure difference between the two holes made the measurements nearly impossible. Although a definite variation in the pressure difference was evident from the measurements, the technique was deferred to a later study.

Pitot pressure probe– The probe (fig. 3(a)) was a flat-nosed boundary-layer probe, which was offset to produce a minimum of interference at the point of measurement. The total pressures were measured with a capacitive pressure transducer.

Laser velocimeter– A schematic of the laser velocimeter is shown in figure 3(b). More detailed descriptions of laser doppler techniques may be found in the literature; for example, references 2–5 with a discussion of a two-color, dual-beam system in reference 5. The laser velocimeter, which was under development during the present tests, is a two-color, dual-beam system that operates in the forward scatter mode with the interference fringe planes in a mutually perpendicular orientation. Two frequencies (with 488.0- and 514.5-nm wavelengths) of a 4-watt, argon-ion laser are utilized. For the present tests, however, only one system of fringes was used. These fringes were aligned normal to the tunnel axis to measure the axial component of velocity only. The estimated diameter

of the measuring point was 0.02 cm, which was roughly the same as the total-pressure-probe height. For the present study, water-condensation particles were used as the scatterers at the higher Mach numbers. For the lower Mach numbers, it was possible to observe naturally occurring dust particles in sufficient numbers to determine the mean velocity. The number of dust particles could be greatly increased by tapping on the filter. The filter appears to limit particle size to at least the micron (μm) range. For the present tests, the doppler signal was analyzed with a Hewlett-Packard 8553B spectrum analyzer and 8443A tracking generator. The various controls of the instrument were adjusted to give the best presentation of the doppler signal. In general, a bandwidth of 100 kHz with a scan width of 1 MHz/cm and a scan time of 1 msec/cm were selected.

The doppler frequency was determined by visually selecting the most probable frequency of occurrence of the signal. Thus, the present measurements were restricted to mean-flow data and are subject to some uncertainties in readability. The major difficulty in reading occurs in the inner part of the boundary layer, where turbulence causes a broad doppler-frequency spectrum.

Hot-wire probes– Figure 4(a) is a sketch of the hot-wire probes used in the present study. A single horizontal wire approximately 0.076-cm long, was used for the longitudinal velocity evaluation. The X-wire probe, with one wire placed normal to the flow and the second wire mounted at 40° to flow, was used to obtain both vertical and longitudinal velocity as well as shear stress data. The wire materials were 0.001-cm-diam platinum/20-percent iridium and platinum/8-percent tungsten, respectively. These wires were easy to mount with soft solder, and strong enough to last through surveys at 0.9 Mach number. The platinum/8-percent-tungsten wire is slightly more velocity sensitive than the platinum/20-percent iridium. Details of the calibration and data-reduction procedure for these probes are given in the appendix. The constant temperature technique (ref. 6) was used for all fluctuating measurements.

Split-film sensors– A recent development in anemometry is the "split film" sensor. This sensor consists of a 0.015-cm-diam quartz rod with two independent films, each covering approximately one half of the cylinder (fig. 4(b)). Film number 1 covers the top half of the cylinder and film number 2 covers the lower half of the cylinder. The sum of the heat transfer from the two cylinders is expected to be similar to that of the completely coated cylinder. Thus, the total heat transfer will give a result much like that of a horizontal hot wire. Each half of the split-film sensor will respond to both the flow magnitude and its direction, much as a yawed hot wire. The split-film sensor has the advantage that the complete sensor has a spacing of only 0.015 cm in the vertical direction. Details of the evaluation of the split-film output are covered in the appendix.

EXPERIMENTAL RESULTS

The results of the investigation reported herein are presented in two sections. The first section describes the mean-flow measurements and presents additional data required for hot-wire and split-film calibration measurements and turbulent shear-stress evaluation. The second section pertains to the turbulence measurements and includes evaluations of the split-film sensor as well as the results of an investigation into the sources of error encountered when measuring shear stress and vertical velocity fluctuations with an X-wire probe.

Mean-Flow Measurements

Channel centerline measurements– Figure 5 shows the variation of the centerline Mach number as a function of the ratio of local wall static pressure to the inlet atmospheric (stagnation) pressure. The difference between the measured curve and the adiabatic relation is due to the losses across the filter, honeycomb, and screen. The filter accounts for the major portion of the loss. The effect of probe blockage can be seen at the higher Mach numbers (above $M_\infty \cong 0.75$) where the laser measurements in the probe-free channel give a higher Mach number for a given pressure ratio.

Figure 6 is a direct comparison of the channel centerline velocity measurements simultaneously obtained from the laser velocimeter and the two different total pressure probes. The static pressure was measured by a wall tap directly below the total pressure probe. Total pressure probe number 2 is the one shown in figure 3. Probe number 1 is similar to probe number 2, but did not have an offset. All of the velocity profile measurements were made with probe number 2. Both probes show a slight deviation from the laser data for velocities above 285 m/s. Probe number 1 shows the larger effect and was not used in further measurements. Although considerable condensation occurs at the higher Mach numbers, no evidence of an effect on the total pressure measurements was found. The good agreement between the total pressure probe and the laser measurements along the centerline indicates that both techniques were giving correct mean-flow information.

Surface-pressure measurements– Figure 7 shows the static pressure drop along the test section wall for different Mach numbers. The pressure gradients shown are quite large. The equivalent pressure gradient for a fully developed channel flow with the same centerline conditions would be 1/2 to 1/3 of those shown in figure 7.

Flow-field surveys– To obtain velocity and Mach number profiles from pitot pressure measurements, it was assumed that static pressure and total temperature were constant across the boundary layer. The influence of the total pressure probe on the wall static pressure adjacent to the probe tip is shown with an expanded vertical scale in figure 8. Two effects are noted: first, the local effect of the probe tip during the first 0.5 cm of travel away from the wall; the second, the blockage effect on the wall pressure as the probe continues into the flow. The error in flow Mach number caused by both effects is less than 1 percent, including the variation in total pressure during a test caused by the atmospheric inlet.

A set of mean-flow profiles were taken for the complete range of channel Mach numbers. The survey results, tabulated in table 1, were made on the top wall at the location of static tap number 3 (fig. 1). Figure 9 shows typical mass-flow profiles. The effect of Mach number and pressure gradient on the profiles is almost negligible.

Figure 10 compares the mean velocity profile measured with the laser with that measured with the total pressure probe for two Mach numbers. For the second case, at $M_\infty \approx 0.9$, a small difference between the results from the two instruments is observed. The laser velocimeter shows more uncertainty because of the turbulence effect on the spectrum, but it also consistently indicates slightly higher values of U/U_e. It is believed that this may have been caused at this high Mach number by blockage effects during the probe tests. Also, the technique used to evaluate the laser data for the present tests results in the modal velocity being recorded, whereas the probe data represent the mean velocity. Additional tests that include an investigation of particle seeding distribution would be required to resolve these differences. Comparisons at lower Mach numbers

indicated excellent agreement. The overall good agreement between the two measurements at Mach numbers less than 0.75 indicates both techniques give correct mean-flow information. Figure 11 presents a plot of the mass-flow profile parameters: displacement thickness, momentum thickness, form factor, and momentum thickness Reynolds number.

Surface-skin friction– Figure 12 shows measured values of the local skin-friction coefficient. Placing the probe in the channel (tip on centerline) produced a slight difference, as shown by the dashed curve. The data are compared with several empirical relations (refs. 7–9). The compressible corrections to these relations were calculated according to the method outlined by Rubesin and Inouye (ref. 10). The plotted results show that none of these relations give the correct trend with Mach number. The Ludwieg-Tielemann relation (ref. 9), which has been shown to hold for incompressible pressure gradient flows, deviates further from the data than the flat-plate relations of references 7 and 8. The surface skin friction appears to vary directly with the pressure gradient, suggesting a fully developed flow character. A curve fit of the data as a function of pressure gradient gave the result

$$c_f = -144\delta^* \frac{\partial p}{\partial x} + 0.130$$

where δ^* is in meters and $\partial p/\partial x$ is in Newtons per cubic meter.

Transformed velocity profiles– Figure 13 shows a plot of the velocity profiles obtained from total pressure measurements in the logarithmic "similarity" coordinates. The transformation of Van Driest (ref. 11) to account for compressible temperature variations was applied to all the measurements. The deviation from the normal logarithmic profile is similar to that reported by Narashimha and Sreenivasan (ref. 12) for highly accelerated flow. Apparently, the logarithmic representation is questionable for highly accelerated flows. The flow is, of course, approaching a fully developed channel flow, so it should be viewed as an entrance flow rather than a boundary-layer flow.

Turbulence Measurements

Both hot-wire and hot-film anemometer techniques were employed for the measurement of turbulence. As was previously noted, the main objectives of this portion of the investigation were to evaluate the split-film probe in higher speed air flow (all previous work has been done in water or in air at velocities less than 25 m/s) and to isolate the problems encountered in measuring turbulent shear stress near surfaces at high speeds. Therefore, the present measurements are limited mainly to $M_e \approx 0.2$ (i.e., 100 m/s) to avoid major compressibility effects. At this Mach number, it can be assumed that the wire and split-film outputs are only sensitive to velocity fluctuations. The probes were operated at constant resistance overheat ratios of approximately 1.2.

Turbulence intensities– A single-wire probe was employed to measure the free-stream turbulence level of the channel. The measurements assumed negligible total temperature fluctuations. Figure 14 shows the values obtained as a function of free-stream Mach number. Above a Mach number of 0.65, the effects of condensation made it impossible to obtain calibration data. The turbulence levels are somewhat high for wind-tunnel flows (ref. 1), but perhaps not unreasonable for the initial states of channel flow.

Figure 15 shows the normalized longitudinal velocity fluctuations obtained from the split-film and the hot-wire measurements. The vertical wire data were obtained from the vertical wire of the X-wire probe. The film and wires were directly calibrated from measurements of the mean velocity distribution across the boundary layer. The results obtained from the split film are in good agreement with the horizontal wire data. Both agree well with previous incompressible data (ref. 13). Some uncertainty may exist near the surface for the split-film data because of the velocity gradient effect (discussed subsequently) and the calibration uncertainty (see appendix). Turbulent- and mean-velocity gradient effects produced significantly lower results from the vertical wire.

An attempt to correct the vertical wire data for mean velocity gradients can be made as follows: Figure 16 is a plot of the vertical-wire voltage output versus the mean velocity at the center of the wire. The "bars" shown for each point represent the velocity at the top and bottom of the wire. The open symbols shown on figure 15 were obtained using a sensitivity ($S_{un} = dE/dU$) obtained by drawing a smooth curve through the center points shown on figure 16. The variation in sensitivity with velocity obtained in this "direct" type of evaluation is much greater than would be expected from wire heat-loss information (ref. 6). As a second approximation, we fitted a "King's law" to the data through the entire boundary layer, using only the minimum velocity points near the wall (dashed line in fig. 16). The results from this calibration are shown by the solid symbols in figure 15. A slight improvement is noted. As a third approximation, we used the outer region of the boundary layer ($y/\delta > 0.53$) to evaluate the hot-wire sensitivity. Although subject to questionable accuracy (ref. 6), a "King's law" was fitted to the data in the outer region only (solid line in fig. 16). The results, using the outer region sensitivity to the inner part of the layer, are shown as the "tailed" points on figure 15. A marked improvement in the vertical wire indication of the turbulence level is obtained with the extrapolated calibration. However, the corrected vertical wire data are still low.

As pointed out by Sandborn (ref. 6), two different effects contribute to the vertical wire error. The mean velocity gradient just considered makes it extremely difficult to determine the effective sensitivity of the wire. The sensitivity, S_{un}, increases as the velocity along the wire decreases. Also, as found by Gessner and Moller (ref. 14) the temperature of the wire (even for constant temperature operation) is greater at the low velocity end, which increases the sensitivity even more. Thus, the sensitivity becomes a complex function of the wire length. A second important problem is associated with the variation of the turbulent velocity fluctuations across the vertical wire. The variation of the turbulence, coupled with the variation in sensitivity along the wire, makes analytical evaluation extremely difficult. The correction approach employed by Tieleman and Sandborn (ref. 15) was to assume that the vertical-wire rms voltage should be corrected to produce the horizontal-wire velocity value. This correction is equivalent to altering the vertical-wire sensitivity to produce the correct value. Differences between the vertical- and horizontal-wire measurements for the flow evaluated by Tieleman and Sandborn were, at most, only 10 percent. The low-speed results (ref. 15) were found to give too high a value for $\langle u \rangle$ from the vertical wire, whereas the results of the investigation reported herein give values that are too low. The difference between the two results has not been explained. However, it is obvious that the error is much more pronounced for the higher-speed flows.

While the problem of the vertical wire measurement can be eliminated by using only horizontal wires, measurement of the vertical velocity requires a yawed wire that has a finite vertical length. It was hoped that the vertical wire could be employed as a correction for the gradient effect. It is not obvious that the gradient effects on the vertical and yawed wire will be the same. The most direct

improvement would be to reduce the probe size and wire length so that the gradient across the wire is very small. However, it appears impossible to reduce the size sufficiently to eliminate the error.

Figure 17 shows the normalized vertical velocity fluctuations obtained from the split-film and the X-wire measurements. We obtained the X-wire results by using the outer region King's law calibration, as previously described. While the corrected X-wire results compare favorably with previous incompressible results, the split-film data are slightly lower in the region $0.1 < y/\delta < 0.5$. Again, calibration uncertainties could cause these differences.

Turbulent shear stress– To provide a standard for evaluating the shear-stress measurements, the total shear-stress distribution across the boundary layer was computed from the balance of the equations of motion. Mean velocity profiles were measured at static tap stations numbers 1 and 3 (fig. 1) for $M = 0.220$ and 0.504. Figure 18 shows the variation of the mass-flow gradients and vertical mass flow obtained for these two point measurements. The total shear stress was computed from the relation:

$$\partial\tau/\partial y = \rho U \frac{\partial U}{\partial x} + \rho V \frac{\partial U}{\partial y} + \frac{\partial p}{\partial x}$$

The value of ρV was obtained from the measured value of $\partial\rho U/\partial x$ and the continuity equation. Figure 19 is a plot of the evaluated total shear distributions. Note that it was required that $\tau/\tau_w = 0$ at $y/\delta = 1$. This boundary condition requires that the value of $\int_0^\delta (\partial\tau/\partial y)\mathrm{d}y = \tau_w$. For $M_\infty = 0.220$, the value of τ_w was found to be 9.91 N/m^2, as compared to a value of 8.6 N/m^2 measured by the floating element. Thus, the momentum balance gives an uncertainty of 15 percent. For $M_\infty = 0.504$, τ_w, from the momentum balance, was 45.7 N/m^2, while the direct measured value was 42.9 N/m^2 – an uncertainty of 6 percent. The distributions of τ indicate an approach to a near linear variation, which is expected in fully developed flow.

Figure 20 shows the normalized shear stress data obtained from the split-film and X-wire measurements. The solid curve is the $M_e = 0.22$ total shear-stress curve given on figure 19. For the X-wire results, the open symbols represent uncorrected data. We calculated the tailed symbols by using a "King's law" extrapolation of both the yaw and vertical wires from the outer-region calibration. The improvement in the measurements, compared to the expected values, indicates that the velocity gradient across the wires produces a major error in the measurements.

The solid points are a correction applied to the measurements to account for the difference between the vertical- and horizontal-wire results. The correction consisted of changing the vertical-wire sensitivity in order to produce the correct value of the longitudinal turbulent velocity. The same percentage correction was applied to the yaw-wire velocity sensitivity. The correction improves the agreement, but is still not adequate in the region very close to the surface. This correction may be adequate for small mean-flow gradient errors, but it apparently cannot account for errors (caused by the turbulent velocity gradients) in the cross correlation, $\overline{e_u e_v}$. The very large errors near the wall may be due to the inability to correct the correlation values.

In the outer portion of the boundary layer, both the split-film and corrected X-wire results compare favorably with the expected results. Since the momentum balance results were obtained several centimeters upstream of the shear-stress measurements, it appears that the actual momentum-balance distribution may have been slightly different at the measurement station, especially in the outer half of the boundary layer. Near the surface, the split-film results are

questionable. The uncertainty in the calibration, discussed in the appendix, coupled with the gradient effects, may lead to large errors, although the results appear to be an improvement over the hot-wire probe data. While it appears doubtful that the velocity gradient errors can be completely eliminated from the measurements, the split-film sensor provides significantly less error than the uncorrected hot-wire probe. It appears that further evaluation of the sensor at higher Mach numbers is justified.

CONCLUDING REMARKS

Both the mean-surface and flow-field quantities have been documented for a subsonic channel flow at Mach numbers ranging from 0.2 to 0.9. By comparing the mean velocity measurements obtained with pitot probes and a laser velocimeter, we determined that probe interference effects are negligible for Mach numbers less than 0.75. We evaluated hot-wire and split film probe measurements of the turbulent flow field at a channel Mach number equal to 0.22. The split-film sensor proved to be a useful device for obtaining fluctuating measurements. Near solid surfaces, however, a major difficulty in the measurement of turbulent shear stress and vertical velocity is a vertical-space resolution limitation of the probe. For an X-wire probe, these errors, which are due to a space-resolution limitation, make the measurements unacceptable. A suggested correction technique, which significantly improves the X-wire results, is presented. The split-film sensor reduces the space-resolutions errors except for regions very close to the surface.

APPENDIX

X-Wire Probe

The X-wire probe shown in figure 4 is a modification of the standard technique. One wire is placed normal to the flow and the second wire is mounted at approximately $\phi \cong 40^\circ$ to the flow. The vertical wire, being normal to the mean flow, is sensitive to the longitudinal turbulent velocity component, u, only. This vertical wire was found by calibration to be insensitive to flow angles of $\pm 5^\circ$, which are much greater than those encountered in typical boundary layers. The second wire is sensitive to both the longitudinal and vertical velocity, v, components. The output voltage of the two wires may be written as (neglecting compressibility)

$$\text{(normal)} \quad e_n = S_n u \tag{1}$$

$$\text{(yawed)} \quad e_y = S_u u + S_v v \tag{2}$$

where $S_n = \mathrm{d}E_n/\mathrm{d}U$, $S_u = \mathrm{d}E_y/\mathrm{d}U$, and $S_v = (1/U)(\mathrm{d}E_y/\mathrm{d}\phi)$ are the wire sensitivity constants determined from mean flow calibration. S_n and S_u were obtained by traversing the boundary layer and comparing the mean-wire voltage with the measured mean-velocity profiles. The wire sensitivity to angle or vertical velocity, S_v, was obtained by a special calibrator which allowed the wire to be yawed through small angles near the center of the channel. The lowest free-stream velocity that could be obtained was approximately 64 m/s because of limitations in the channel speed regulator. It was assumed that the ratio of the longitudinal-to-vertical velocity sensitivity is a constant which is independent of the local flow velocity. This assumption is implied in nearly all of the yawed-wire head-loss empirical relations (ref. 6). Experimental evidence is given by Sandborn (ref. 6) which indicates a slight second-order variation in the ratio. The present range of calibration was too limited to evaluate any possible variation. The ratio of the sensitivities for the present wires was found to be

$$\frac{S_{v_y}}{S_{u_y}} = 1.30 \pm 0.4 \tag{3}$$

The product of the two wire voltages is:

$$\overline{e_n e_y} = S_n S_u \overline{u^2} + S_n S_v \overline{uv} \tag{4}$$

Thus, the product can be related to the turbulent shear stress, $\overline{uv}$, once $\overline{u^2}$ is determined from the normal wire output.

It appeared that this modified cross-wire technique would be more accurate than the usual crossed-wire methods. The longitudinal component, $\overline{u^2}$, is the most accurate measurement that can be made with the hot wire. Thus, it is only necessary to solve equation (4) for $\overline{uv}$, rather than solving two experimental equations for $\overline{uv}$ and $\overline{v^2}$ (required for conventional crossed wires). The vertical wire also is a direct check on the effect of space resolution of the X-wire probe, since it can be compared directly with a horizontal wire probe.

Split-Film Sensor

The basic operation of the split-film sensor is quite similar to the X-wire, hot-wire anemometers. The sum of the heat transfer from the two films is similar to the total heat transfer observed with a horizontal hot-wire sensor. Figure 21 shows the variation of the "squared sum voltage,"

$$E_S^2 \equiv S_1 E_1^2 + S_2 E_2^2 \tag{5}$$

with velocity for the sensor. Also shown on figure 21 are the individual variations for the films. The coefficient, S, is

$$S \equiv \frac{R_a \alpha}{R(R - R_a)} \tag{6}$$

where α is the thermal coefficient of resistance of the film used ($\alpha = 3.78 \times 10^{-3}$/K), R_a is the resistance of the unheated film, and R is the heated resistance of the film.

A detailed analysis of the split-film sensor was originally given by Spencer and Jones (ref. 16). As with many aspects of turbulence measurements, it was desirable to obtain direct output of each component of the turbulent velocity. The suggestion was made that either the difference in heat transfer or the ratio of the heat transfer could be used to evaluate the flow direction variations. Although evidence was presented to suggest that the difference and the ratio depend only on the flow angle and not the flow velocity, these results are questionable over large velocity variations. Attempts to employ the difference and ratio to evaluate the vertical velocity and the turbulent shear stress for the $M_e = 0.22$ boundary layer proved questionable. The major problem was the slight sensitivities of the difference and the ratio to the mean velocity variation. While the present results are for high-speed flow, a reevaluation of the measurement in low-speed water flow shows similar results. It was concluded that the direct approach of treating the films individually was the most accurate means of evaluating the turbulent shear stress.

The evaluation of the u-component of the turbulence was done in a manner similar to the technique used for horizontal hot wires (ref. 6). The linearized perturbation analysis gives

$$u = \frac{dU}{dE_S} e_S \tag{7}$$

where the fluctuation voltage, e_S, is given as

$$\overline{e_S^2} = \frac{1}{E_2^2}\left(S_1^2 E_1^2 \overline{e_1^2} + 2S_1 S_2 E_1 E_2 \overline{e_1 e_2} + S_2^2 E_2^2 \overline{e_2^2}\right) \tag{8}$$

The quantities $\overline{v^2}$ and $\overline{uv}$ were computed with the assumption that the outputs of the films can be written as

$$\text{(Film number 1)} \qquad e_1 = S_{u_1} u + S_{v_1} v \tag{9}$$

$$\text{(Film number 2)} \qquad e_2 = S_{u_2} u + S_{v_2} v \tag{10}$$

where the sensitivities are obtained from the linearized perturbation analysis as

$$S_u = \frac{dE}{dU} \tag{11}$$

$$S_v = \frac{1}{U}\frac{dE}{d\phi} \tag{12}$$

Thus, the films must be calibrated as a function of the mean velocity, U, and the flow direction indicated by an angle, ϕ. The sensor was calibrated on the centerline of the channel by using a special jig that allowed the probe to rotate ±10° about the axis of the sensor. Typical angle calibrations of the films are shown in figure 22. The angle sensitivity is nearly linear over approximately ±5°.

The values of $\overline{v^2}$ and $\overline{uv}$ were obtained by employing equations (9) and (10) in their mean-square form to give

$$\overline{uv} = \frac{(\overline{e_1^2}/S_{v_1}^2 - \overline{e_2^2}/S_{v_2}^2) + \overline{u^2}(S_{u_2}^2/S_{v_2}^2 - S_{u_1}^2/S_{v_2}^2)}{2(S_{u_1}/S_{v_1} + S_{u_2}/S_{v_2})} \tag{13}$$

and

$$\overline{v^2} = \frac{(\overline{e_1^2}/S_{u_1}S_{v_1} + \overline{e_2^2}/S_{u_2}S_{v_2}) - \overline{u^2}(S_{u_1}/S_{v_1} + S_{u_2}/S_{v_2})}{(S_{v_1}/S_{u_1} + S_{v_2}/S_{u_2})} \tag{14}$$

The measurements of $(\overline{u^2})^{1/2}$, $(\overline{v^2})^{1/2}$ and $\overline{uv}$ for $M_\infty = 0.22$ boundary layer were made at the rear of the window station. The present calibration was limited to the velocities shown in figure 21, which are not as low as those encountered near the wall. This limitation was imposed by the mass-flow control plates at the channel exit. In order to extrapolate the calibration to the lower velocities, a "King's Law" fit of the calibration curve was employed:

$$E_S^2 = A + B\,U^{1/2} \tag{15}$$

while some questions exist on the accuracy of this relation for predicting the derivatives, dE_S/dU (ref. 6), it may not be too much in error for the large-sized cylinder. The known velocity distribution within the boundary layer was not used because of the possible velocity gradient effect on the heat transfer. It was obvious that, when the probe was very close to the wall the film nearer the wall was at a much lower velocity than that for the other film. Thus the velocity gradient effect across the diameter of the sensor will produce errors near the surface. In addition, such effects as molecular conduction between the lower film and the wall would increase the heat transfer and, thus, the value of E_S.

Since the evaluation of the angle sensitivity was limited in the present study by the velocity limits, it was assumed that the velocity and angle sensitivities were proportional, that is,

$$S_u/S_v = \text{constant} \tag{16}$$

This assumption is implied in nearly all hot-wire analyses of yawed wires (ref. 6). It is, at best, a first-order approximation, which should be replaced by direct calibration, if possible. Figure 23 shows the actual measured values of the angle sensitivities compared with best fits of equation (16). This assumed relation may explain some of the disagreement between the evaluated shear stress and the predicted distribution.

The split-film sensor in the commercial form proved too weak for the present flow conditions. It was necessary to add ceramic cement to the small support to prevent bending in the flow. The bending acts to rotate the sensor, which, in turn, causes a calibration error. The probe was also modified so that the near wall could be surveyed. Near the surface, the hole for the probe is very near the sensor, so that some uncertainty in the measurement can be expected. An attempt was made to fill the hole with putty at the start of each survey.

The sensor has been operated at flow velocities up to 130 m/s without damage, and improvements in support strength should make it usable for much higher velocities. The sensor would appear to be near the minimum limit in usable size. During the course of the study, it appeared that only the newer anemometers with specific hot-film taylored circuits were capable of giving correct outputs. Within the operational limits, it did not appear that variations in the sensitivity coefficients between films produced adverse effects.

REFERENCES

1. Sandborn, V. A.: A Review of Turbulence Measurements in Compressible Flow. NASA TM X-62,337, 1974.

2. Yeh, Y.; and Cummins, H. Z.: Localized Fluid Flow Measurements With an He-Ne Laser Spectrometer. Appl. Phys. Lett., vol. 4, 1964, p. 176.

3. Mazumder, M. K.: A Symmetrical Laser Doppler Velocity Meter and Its Application to Turbulence Characterization. NASA CR-2031, 1972.

4. Fridman, J. D.; Huffaker, R. M.; and Kinnard, R. F.: Laser Doppler System Measures Three-Dimensional Vector Velocity and Turbulence, Laser Focus, vol. 4, no. 21, 1968, pp. 34–38.

5. Grant, G. R.; and Orloff, K. L.: A Two-Color, Dual Beam Backscatter Laser Doppler Velocimeter. NASA TM X-62,254, 1973.

6. Sandborn, V. A.: Resistance Temperature Transducers. Meteorology Press, Fort Collins, Colorado, 1972.

7. Falkner, V. M.: A New Law for Calculating Drag. Aircraft Engineering, vol. 15, 1943, pp. 65–69.

8. Squire, H. B.; and Young, A. D.: The Calculation of Profile Drag of Airflow. Ames Research Center R&M 1838, 1937.

9. Lugwieg, H.; and Tillmann, W.: Investigations of the Wall-Shearing Stress in Turbulent Boundary Layers. NACA TM 1285, 1950.

10. Rubesin, Morris W.; and Inouye, Mamoru: Forced Convection, External Flows. Section 8. Handbook of Heat Transfer, McGraw-Hill, 1973, p. 8–156.

11. Van Driest, F. R.: Turbulent Boundary Layer in Compressible Fluids. J. Aeronaut. Sci., vol. 18, no. 3, 1951, pp. 145–160, 216.

12. Narasimha, R.; and Sreenivasan, K. R.: Relaminarization in Highly Accelerated Turbulent Boundary Layers. J. Fluid Mech., vol. 61, pt. 3, 1973, pp. 417–447.

13. Klebanoff, P. S.: Characteristics of Turbulence in a Boundary Layer with Zero Pressure Gradient. NACA Report 1247, 1954.

14. Gessner, F. B.; and Moller, G. L.: Response Behavior of Hot Wires in Shear Flow. J. Fluid Mech., vol. 47, pt. 3, 1971, p. 449.

15. Tieleman, H. W.; and Sandborn, V. A.: Turbulent Shear Measurements in Large Velocity Gradients. Colorado State University, Engineering Research Center Report CER67-68HWT-VAS68, 1968.

16. Spencer, B. W.; and Jones, B. G.: Turbulence Measurements with the Split Film Anemometer Probe. Proc. Symposium on Turbulence in Liquids. University of Missouri-Rolla, 1971.

TABLE 1.– MEAN FLOW MEASUREMENTS

M_∞ = 0.218	M_∞ = 0.312	M_∞ = 0.399	M_∞ = 0.499
Re_θ = 16400	Re_θ = 21800	Re_θ = 27300	Re_θ = 31800
U_e = 83.6 m/sec	U_e = 114 m/sec	U_e = 146 m/sec	U_e = 181 m/sec
ρ_e = 1.169 kg/m^3	ρ_e = 1.132 kg/m^3	ρ_e = 1.081 kg/m^3	ρ_e = 1.042 kg/m^3
μ_e = 1.813X10^{-5} kg/m sec	μ_e = 1.800 X10^{-5} kg/m sec	μ_e = 1.793X10^{-5} kg/m sec	μ_e = 1.761X10^{-5} kg/m sec
T_e = 293.0 K	T_e = 290.3 K	T_e = 288.9 K	T_e = 282.4 K
p_w = 9.818X10^4 N/m^2	p_w = 9.430X10^4 N/m^2	p_w = 8.963X10^4 N/m^2	p_w = 8.439X10^4 N/m^2
T_o = 292.7 K	T_o = 295.6 K	T_o = 298.1 K	T_o = 296.6 K
p_o = 10.20X10^4 N/m^2	p_o = 10.19X10^4 N/m^2	p_o = 10.17X10^4 N/m^2	p_o = 10.20X10^4 N/m^2
δ^* = 0.433 cm	δ^* = 0.434 cm	δ^* = 0.437 cm	δ^* = 0.437 cm
θ = 0.340 cm	θ = 0.326 cm	θ = 0.333 cm	θ = 0.320 cm
H = 1.27	H = 1.33	H = 1.32	H = 1.37
c_f = 0.0026	c_f = 0.00265	c_f = 0.00268	c_f = 0.00272

y, cm	M	$\frac{U}{U_e}$	y, cm	M	$\frac{U}{U_e}$	$\frac{\rho U}{\rho_e U_e}$	y, cm	M	$\frac{U}{U_e}$	$\frac{\rho U}{\rho_e U_e}$	y, cm	M	$\frac{U}{U_e}$	$\frac{\rho U}{\rho_e U_e}$
0.010	0.112	0.516	0.010	0.166	0.535	0.529	0.010	0.227	0.574	0.561	0.010	0.246	0.501	0.483
.015	.115	.530	.015	.166	.536	.529	.017	.227	.576	.563	.013	.248	.505	.487
.025	.117	.538	.020	.171	.551	.545	.020	.230	.583	.570	.019	.259	.528	.510
.038	.122	.560	.025	.173	.560	.552	.025	.233	.590	.577	.025	.268	.546	.527
.051	.126	.579	.038	.178	.575	.567	.050	.245	.621	.608	.038	.278	.566	.548
.076	.134	.614	.051	.184	.596	.588	.075	.253	.640	.627	.050	.292	.594	.576
.102	.137	.629	.076	.192	.620	.612	.100	.258	.652	.640	.075	.309	.628	.609
.152	.144	.661	.102	.197	.635	.629	.150	.266	.673	.661	.102	.321	.651	.633
.203	.149	.684	.152	.207	.669	.662	.200	.276	.696	.684	.152	.337	.683	.665
.254	.153	.703	.203	.214	.701	.695	.300	.286	.722	.711	.203	.348	.705	.687
.318	.156	.714	.254	.220	.708	.703	.400	.295	.744	.732	.254	.355	.720	.703
.381	.159	.729	.318	.224	.723	.718	.600	.308	.776	.766	.318	.364	.737	.720
.445	.162	.745	.381	.230	.741	.735	.800	.320	.806	.797	.381	.371	.751	.734
.508	.164	.755	.445	.233	.751	.746	1.00	.330	.830	.822	.445	.377	.763	.747
.635	.168	.772	.508	.236	.761	.756	1.25	.340	.856	.849	.508	.382	.772	.756
.762	.173	.794	.76[illegible]	.250	.806	.802	1.50	.350	.881	.875	.635	.392	.791	.776
1.02	.178	.819	1.0[illegible]	.259	.833	.829	1.75	.359	.903	.898	.762	.400	.808	.793
1.52	.191	.877	1.52	.274	.882	.880	2.00	.369	.926	.922	1.02	.415	.837	.823
2.03	.201	.922	2.03	.288	.926	.925	2.25	.376	.944	.941	1.52	.441	.888	.878
2.54	.211	.966	2.54	.301	.966	.966	2.50	.384	.963	.961	2.03	.464	.932	.925
3.05	.217	.993	3.05	.309	.992	.992	2.75	.390	.979	.977	2.54	.483	.969	.965
3.30	.217	.995	3.30	.311	1.00	1.00	3.00	.394	.988	.987	3.05	.495	.992	.991
3.56	.217	.996					3.25	.397	.996	.995	3.30	.498	.998	.997
3.81	.218	1.00					3.50	.398	.998	.998	3.56	.499	.999	.998
							3.60	.399	.999	.999	3.68	.499	1.00	.999
							3.70	.399	1.00	1.00	3.81	.499	1.00	1.00

TABLE 1.– MEAN FLOW MEASUREMENTS – Concluded.

M_∞ = 0.595 Re_θ = 33400 U_e = 214 m/sec ρ_e = 0.9833 kg/m^3 μ_e = 1.742X10^{-5} kg/m sec T_e = 277.7 K p_w = 7.830X10^4 N/m^2 T_o = 296.3 K p_o = 10.20X10^4 N/m^2 δ^* = 0.424 cm θ = 0.297 cm H = 1.43 c_f = 0.00275				M_∞ = 0.728 Re_θ = 31300 U_e = 258 m/sec ρ_e = 0.9024 kg/m^3 μ_e = 1.697X10^{-5} kg/m sec T_e = 269.2 K p_w = 6.991X10^4 N/m^2 T_o = 297.7 K p_o = 10.21X10^4 N/m^2 δ^* = 0.391 cm θ = 0.246 cm H = 1.59 c_f = 0.00280				M_∞ = 0.778 Re_θ = 30100 U_e = 273 m/sec ρ_e = 0.8720 kg/m^3 μ_e = 1.679X10^{-5} kg/m sec T_e = 265.3 K p_w = 6.637X10^4 N/m^2 T_o = 297.3 K p_o = 10.19X10^4 N/m^2 δ^* = 0.391 cm θ = 0.231 cm H = 1.70 c_f = 0.00282				M_∞ = 0.878 Re_θ = 33300 U_e = 303 m/sec ρ_e = 0.8143 kg/m^3 μ_e = 1.634X10^{-5} kg/m sec T_e = 256.6 K p_w = 6.004X10^4 N/m^2 T_o = 296.2 K p_o = 10.18X10^4 N/m^2 δ^* = 0.386 cm θ = 0.231 cm H = 1.67 c_f = 0.00288			
y, cm	M	$\frac{U}{U_e}$	$\frac{\rho U}{\rho_e U_e}$	y, cm	M	$\frac{U}{U_e}$	$\frac{\rho U}{\rho_e U_e}$	y, cm	M	$\frac{U}{U_e}$	$\frac{\rho U}{\rho_e U_e}$	y, cm	M	$\frac{U}{U_e}$	$\frac{\rho U}{\rho_e U_e}$
0.010	0.289	0.497	0.471	0.010	0.417	0.592	0.547	0.010	0.436	0.582	0.529	0.010	0.486	0.550	0.522
.015	.293	.505	.478	.015	.421	.598	.553	.015	.437	.584	.530	.015	.490	.586	.526
.020	.301	.518	.491	.020	.434	.615	.569	.020	.441	.589	.536	.020	.496	.592	.536
.025	.311	.535	.508	.025	.438	.621	.575	.025	.447	.597	.543	.025	.506	.604	.546
.038	.329	.565	.537	.050	.459	.650	.605	.050	.474	.631	.577	.038	.520	.620	.561
.050	.343	.589	.561	.075	.477	.674	.629	.075	.506	.671	.618	.050	.537	.639	.583
.075	.366	.627	.599	.100	.491	.693	.648	.100	.516	.684	.631	.075	.548	.651	.594
.102	.380	.652	.624	.150	.510	.718	.674	.150	.542	.723	.672	.102	.581	.688	.632
.152	.402	.688	.660	.200	.527	.741	.698	.200	.561	.741	.690	.127	.601	.710	.656
.203	.415	.710	.683	.300	.547	.768	.727	.300	.588	.774	.726	.152	.614	.725	.670
.254	.425	.726	.700	.400	.568	.796	.757	.400	.611	.802	.756	.203	.634	.746	.694
.318	.435	.743	.717	.600	.588	.822	.786	.600	.625	.819	.775	.254	.646	.759	.707
.381	.444	.757	.732	.800	.610	.849	.818	.800	.655	.865	.817	.318	.667	.781	.732
.445	.452	.770	.746	1.00	.627	.872	.843	1.00	.674	.878	.843	.381	.682	.798	.752
.508	.459	.782	.758	1.25	.647	.898	.872	1.25	.695	.903	.873	.445	.694	.810	.764
.635	.470	.800	.778	1.50	.663	.918	.897	1.50	.713	.924	.899	.508	.707	.824	.782
.762	.483	.821	.800	1.75	.679	.938	.921	1.75	.730	.944	.923	.635	.723	.840	.794
1.02	.502	.852	.833	2.00	.693	.956	.943	2.00	.744	.961	.945	.762	.738	.857	.819
1.52	.533	.901	.887	2.25	.704	.970	.959	2.25	.756	.974	.962	1.02	.765	.886	.852
2.03	.556	.938	.929	2.50	.715	.984	.976	2.50	.766	.986	.978	1.52	.809	.931	.908
2.54	.579	.975	.971	2.75	.721	.992	.987	2.75	.774	.995	.991	2.03	.843	.965	.953
3.05	.592	.995	.993	3.00	.726	.997	.994	3.00	.777	.998	.996	2.54	.867	.989	.983
3.30	.594	.999	.998	3.25	.727	.999	.998	3.25	.778	1.00	.999	2.79	.873	.995	.989
3.56	0.595	1.00	1.00	3.50	.728	1.00	.999	3.50	.778	1.00	1.00	3.05	.876	.998	.998
				3.60	.728	1.00	1.00	3.60	.778	.999	1.00	3.30	0.878	1.00	1.00

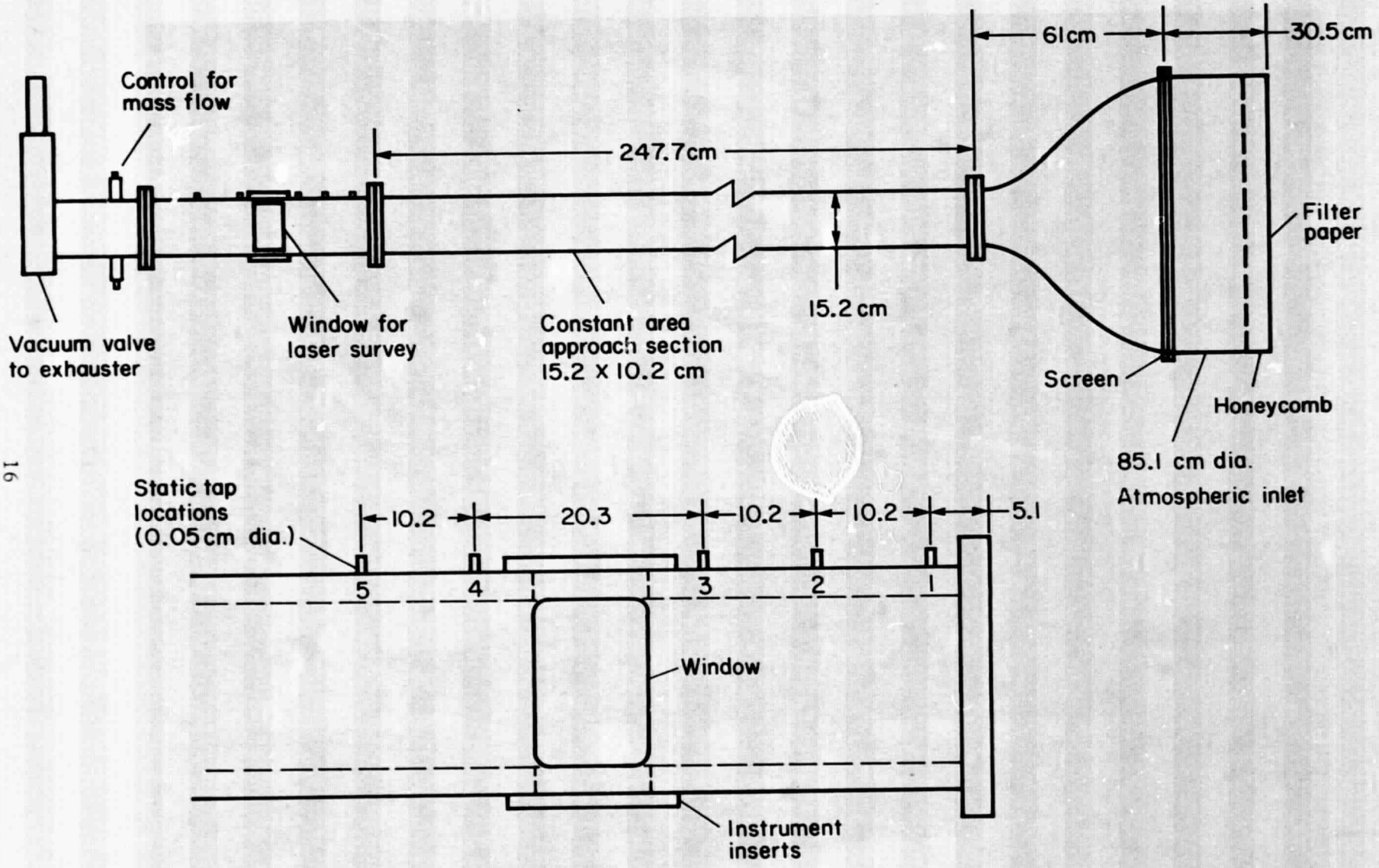

Figure 1.– Schematic of compressible flow channel.

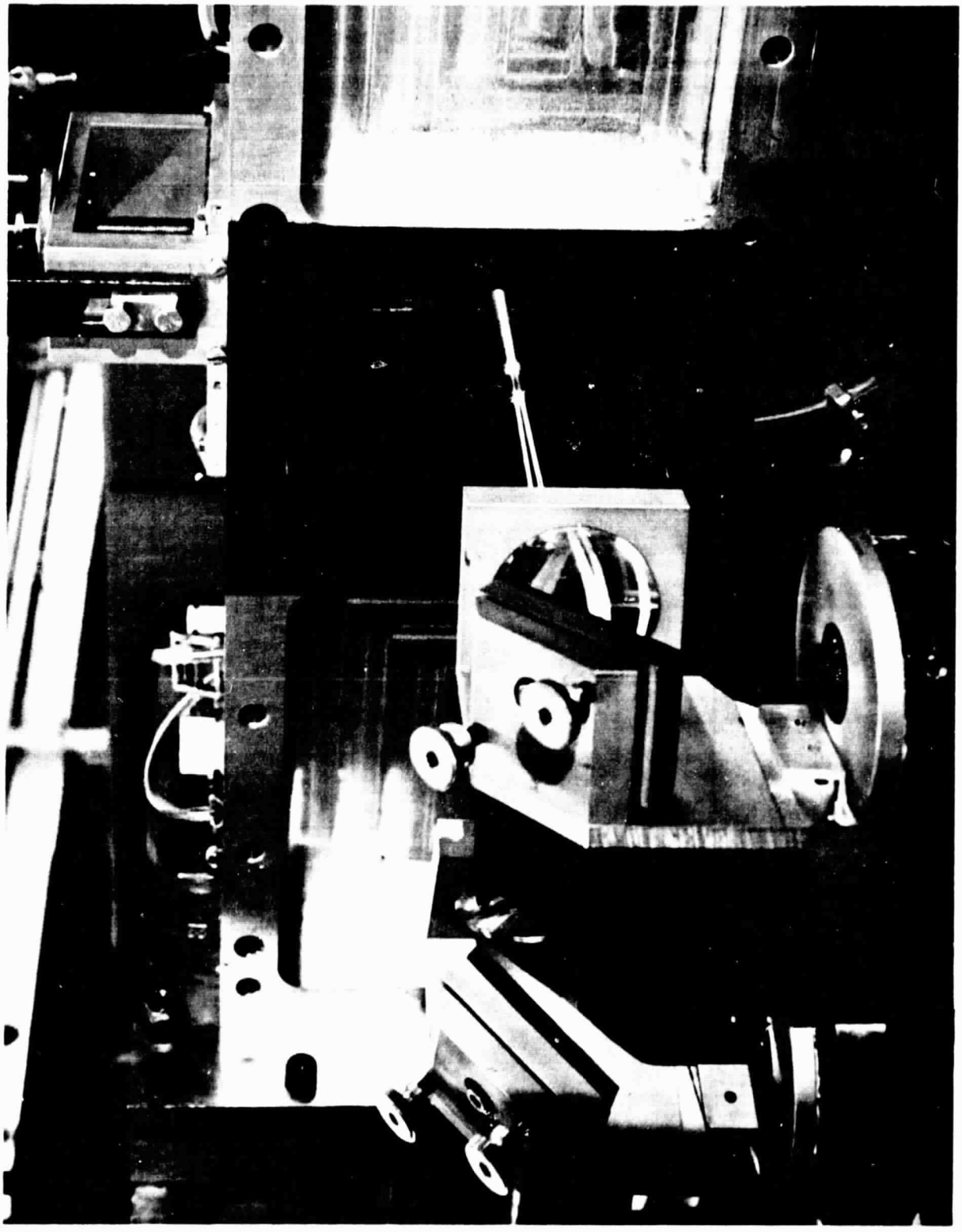

Figure 2.— Photograph of test section and laser beams.

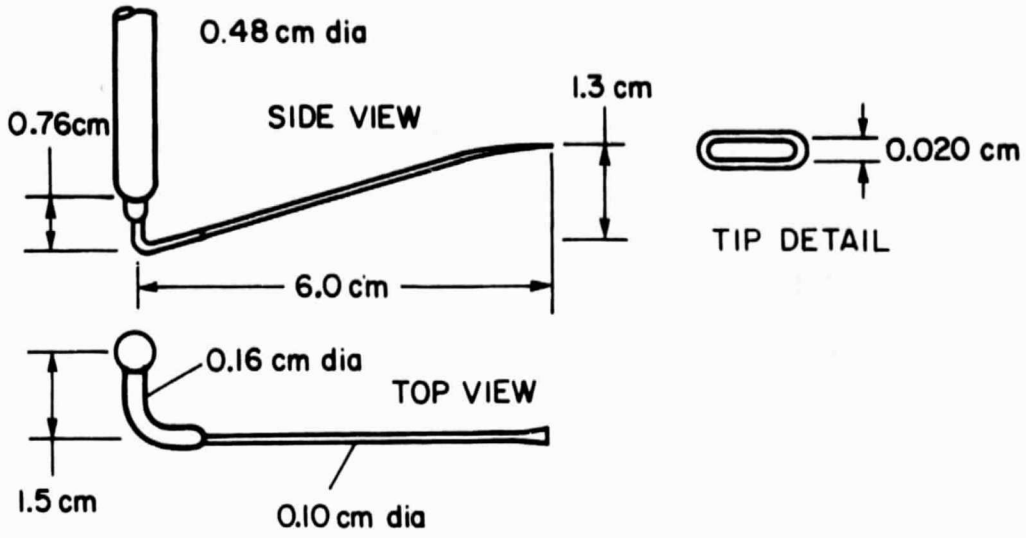

(a) Total pressure probe

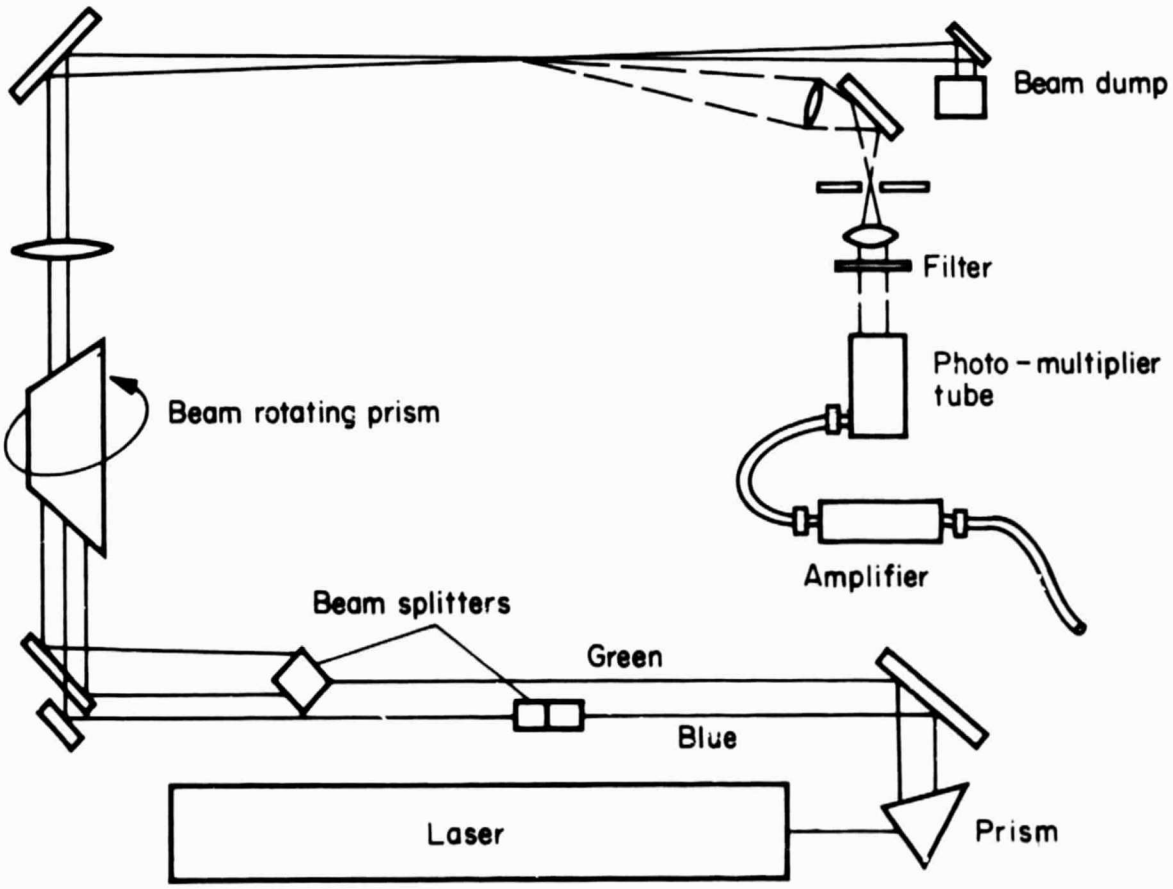

(b) Laser velocimeter schematic

Figure 3.– Velocity instrumentation schematics.

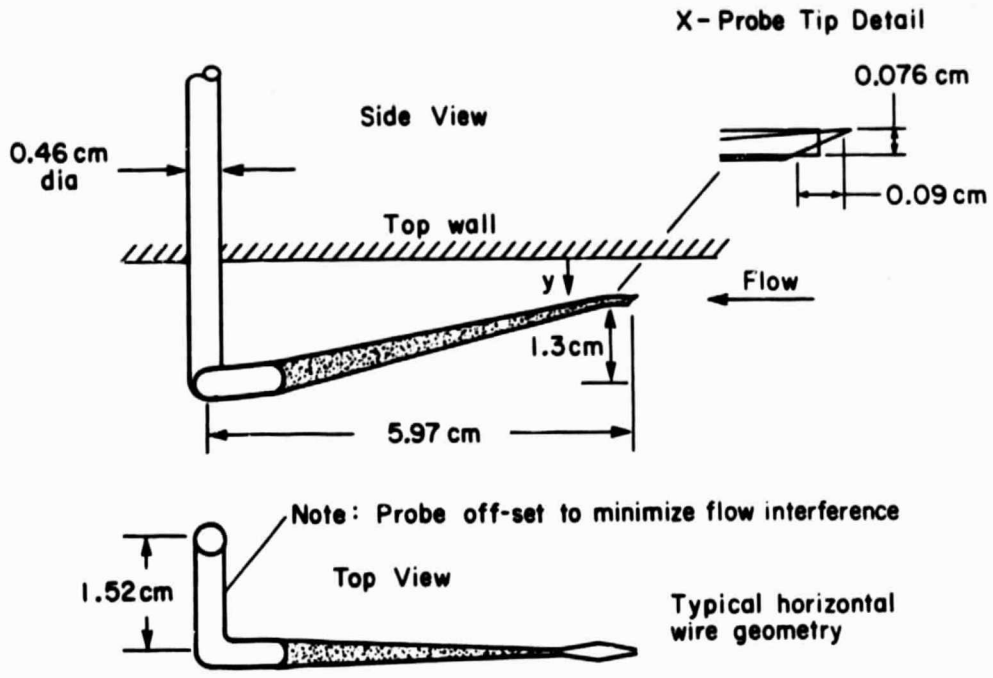

(a) Hot-wire probes.

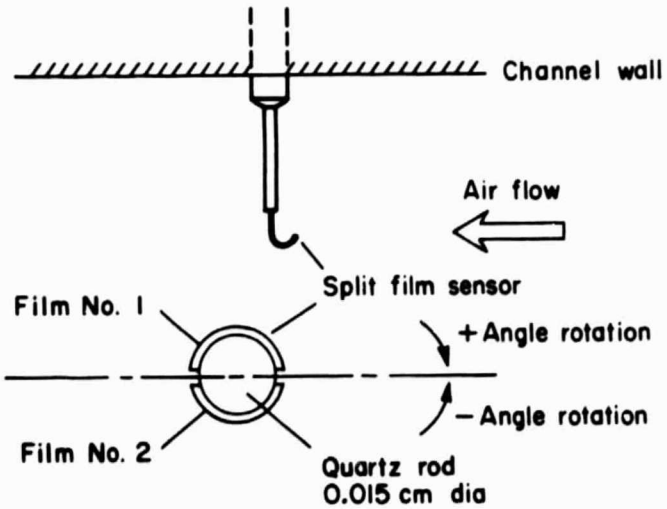

(b) Split-film sensor.

Figure 4.– Turbulence probe geometries.

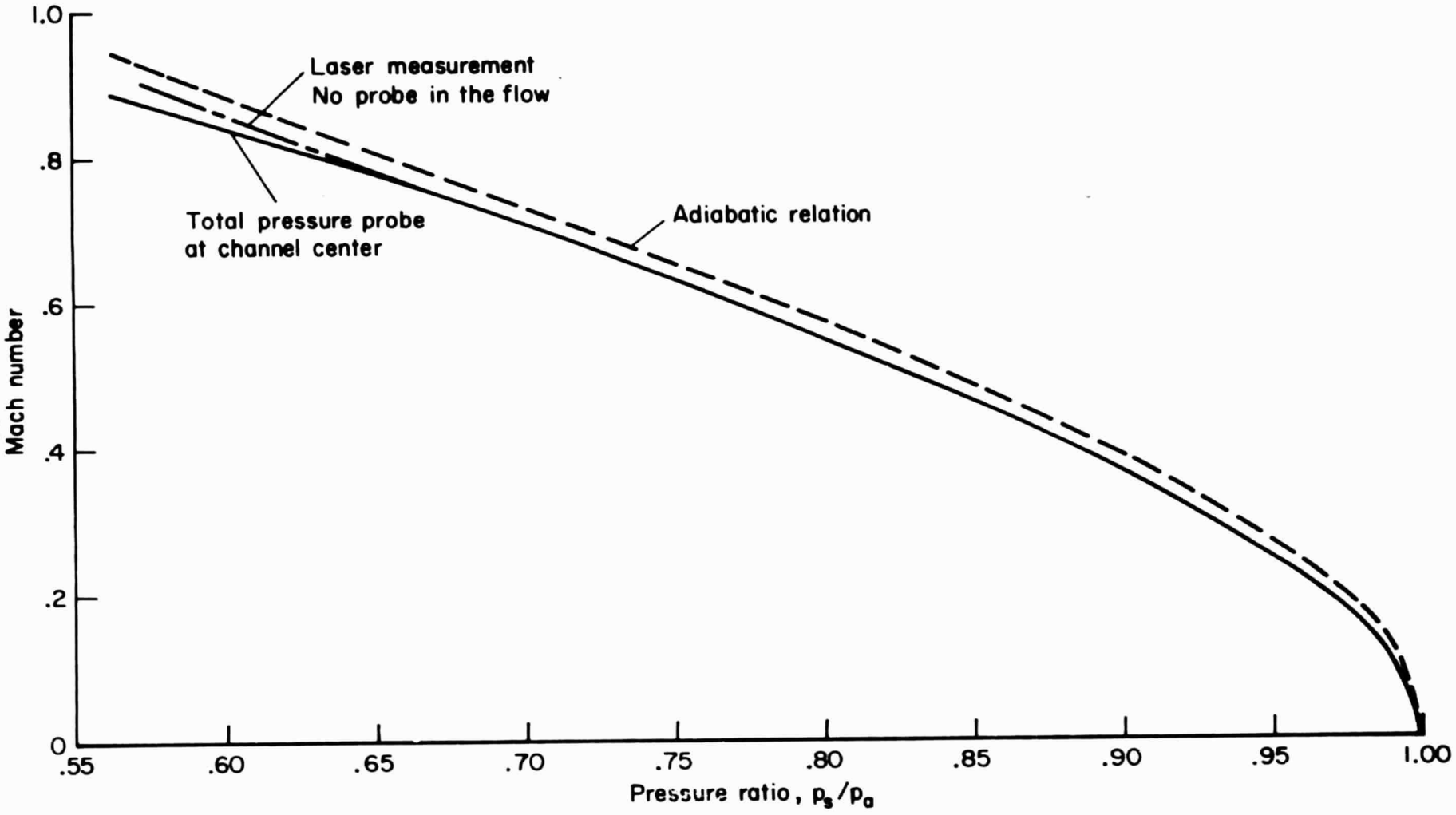

Figure 5.– Variation of channel centerline Mach number at the test section.

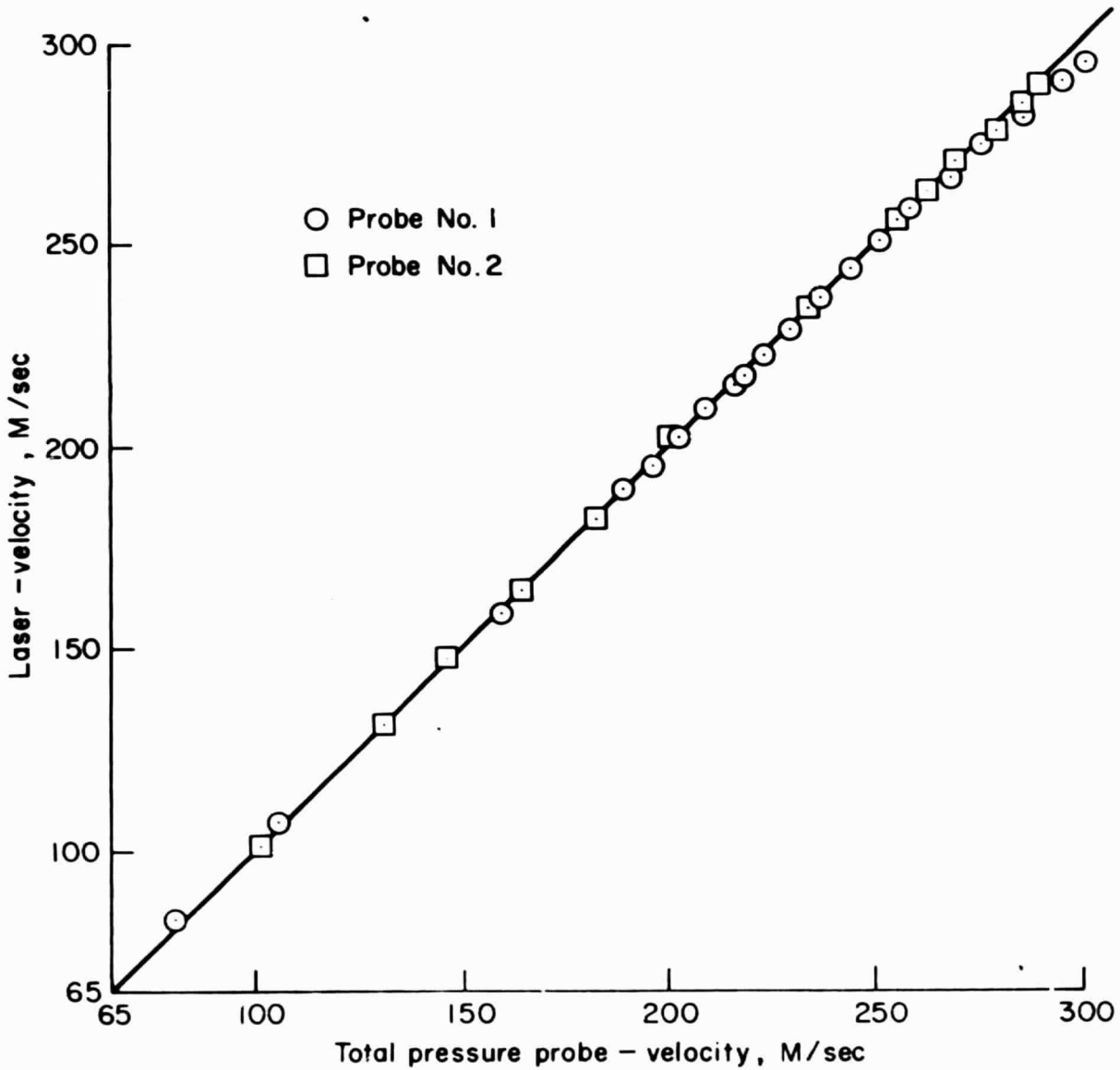

Figure 6.— Comparison of laser-velocimeter and total-pressure-probe measurements.

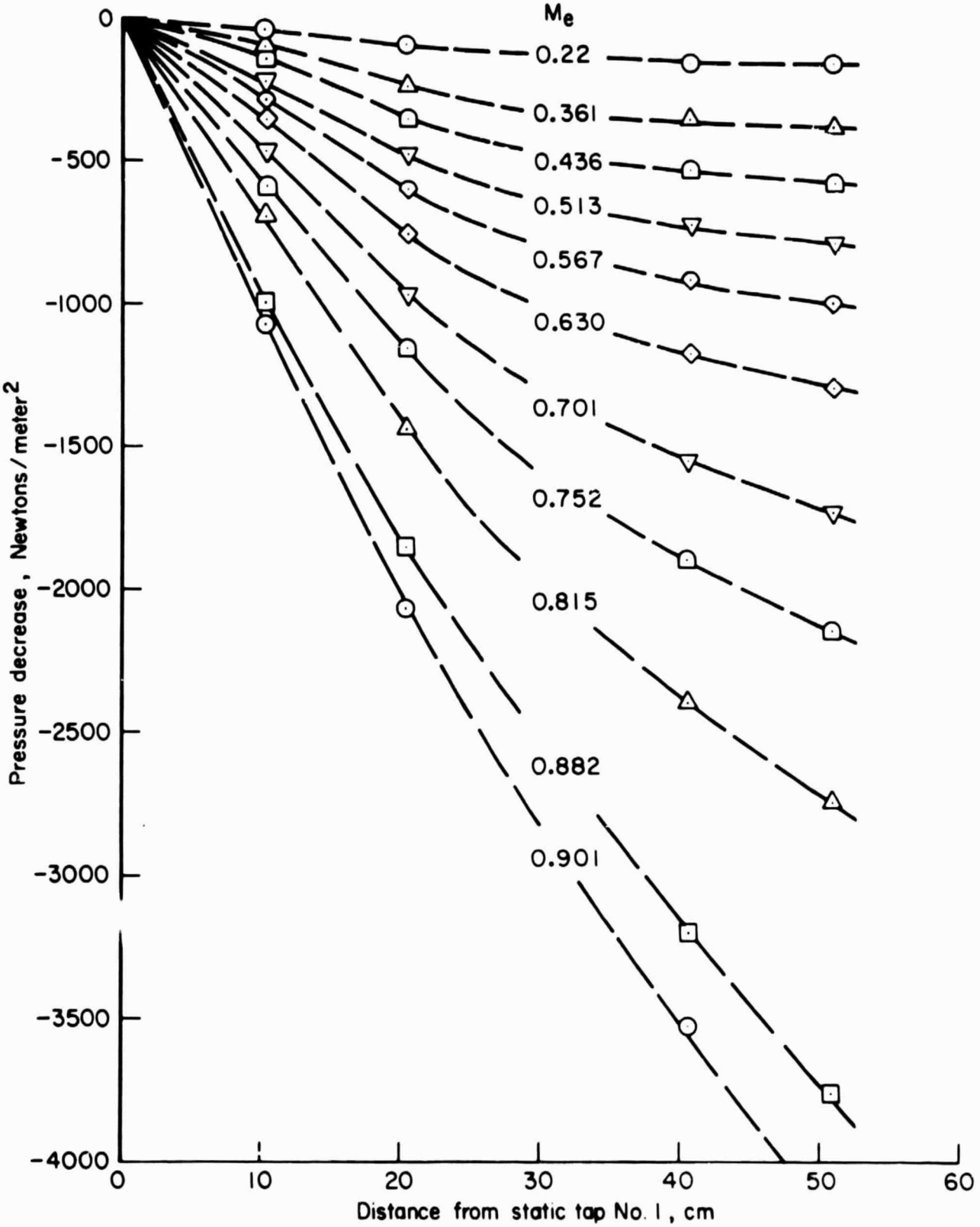

Figure 7.– Static pressure distributions along the channel test section.

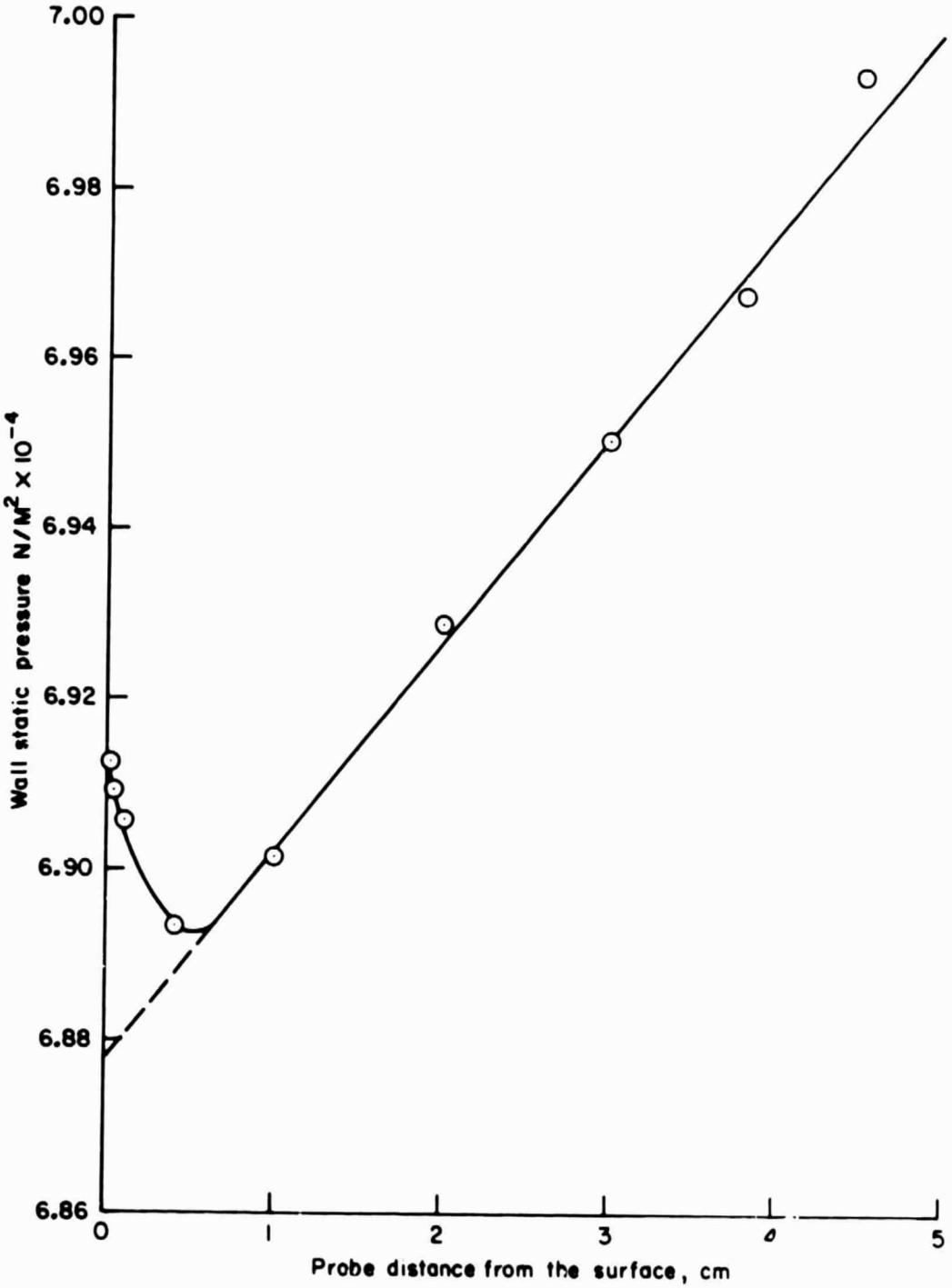

Figure 8.– Probe effect on the local-wall static-pressure measurement, $M_\infty = 0.728$.

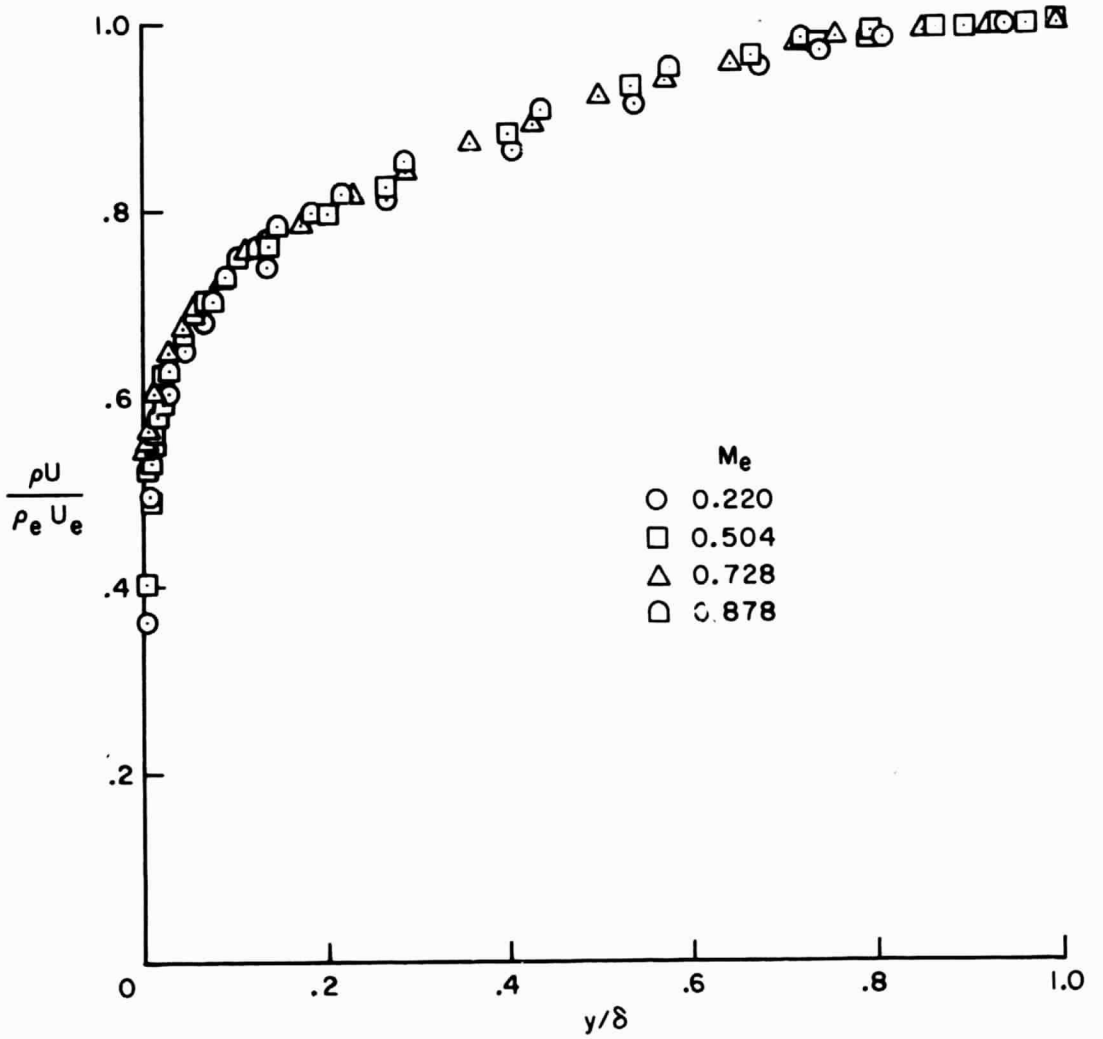

Figure 9.– Mean mass-flow distributions.

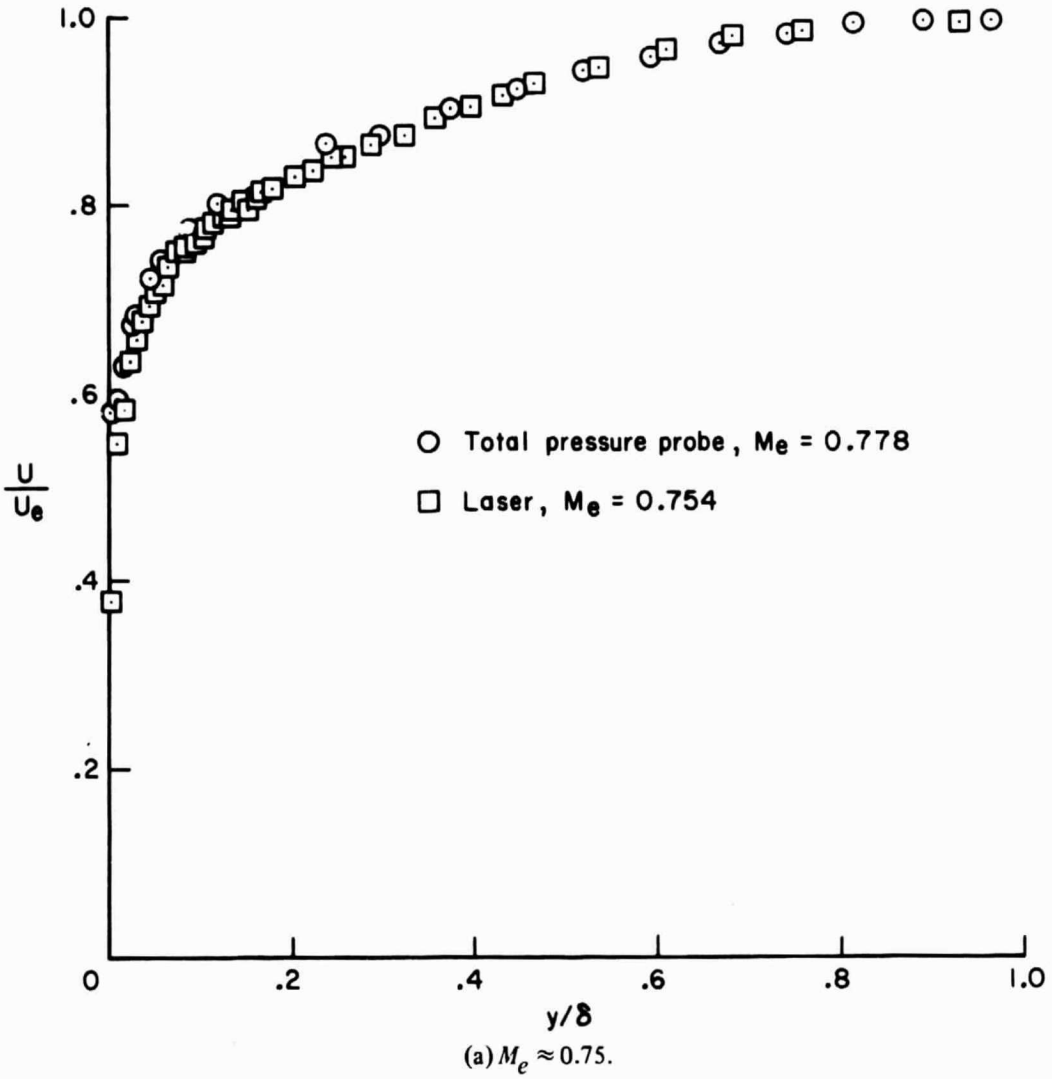

(a) $M_e \approx 0.75$.

Figure 10.– Comparison of laser and total-pressure-probe mean-velocity measurements.

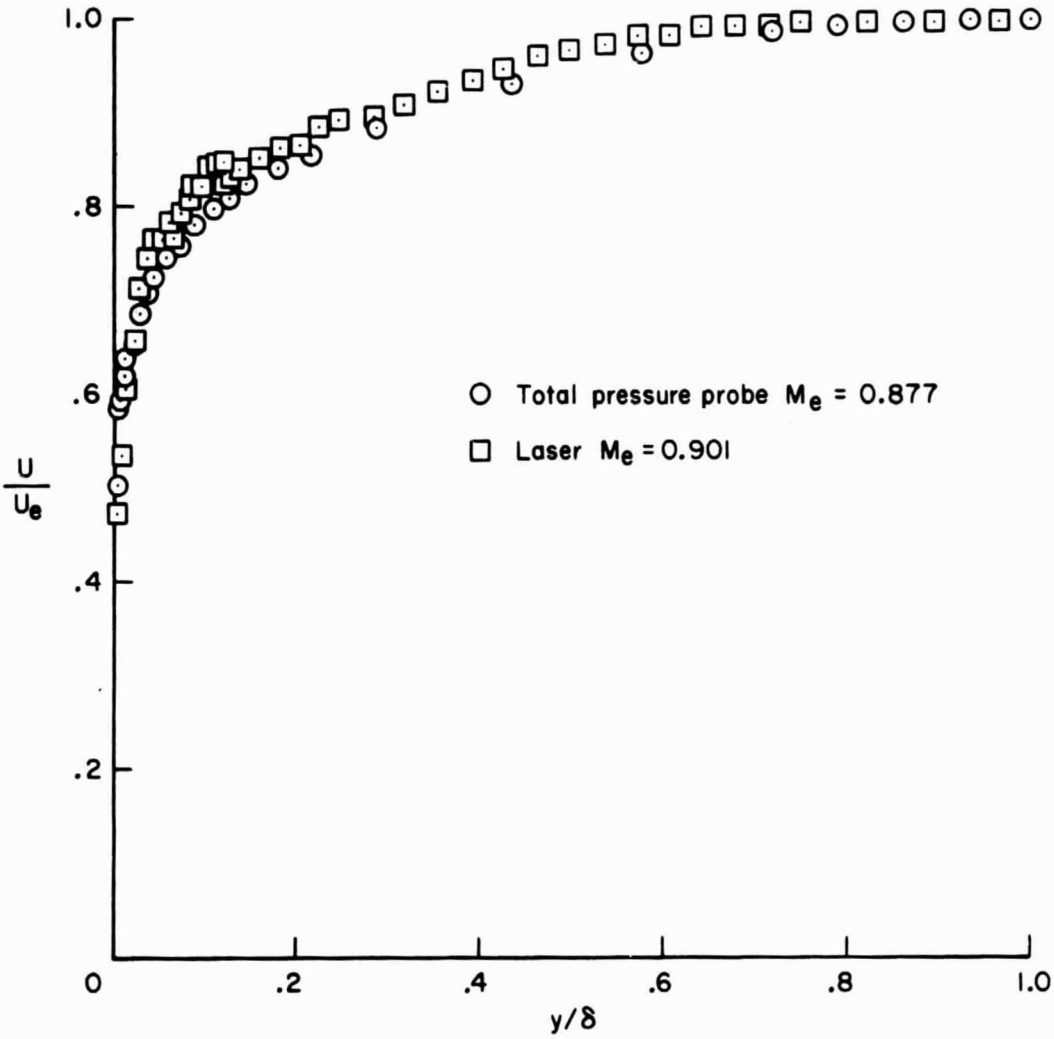

(b) $M_e \approx 0.90$.

Figure 10.– Concluded.

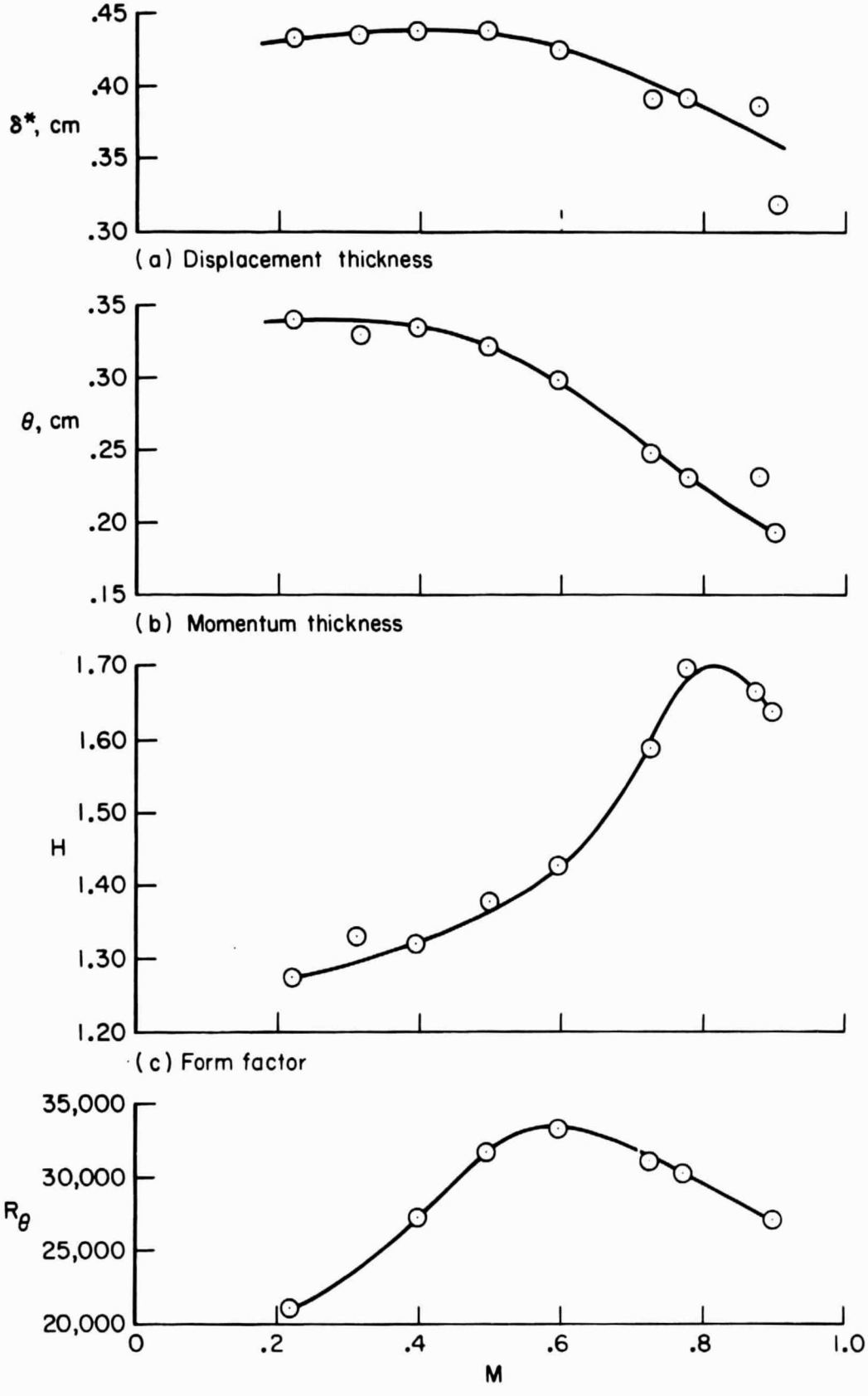

Figure 11.—Channel boundary-layer parameters.

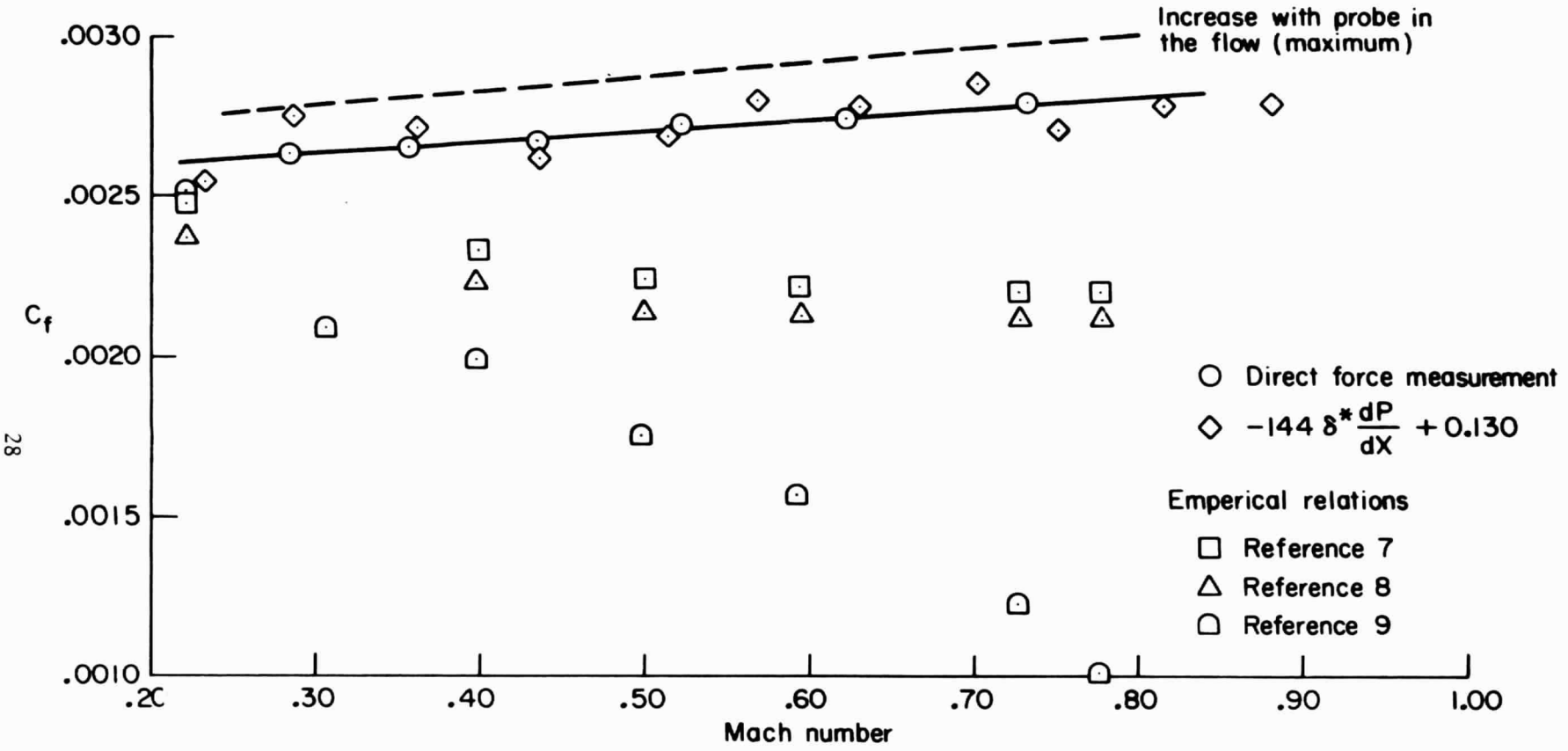

Figure 12.– Skin-friction coefficient variation with Mach number.

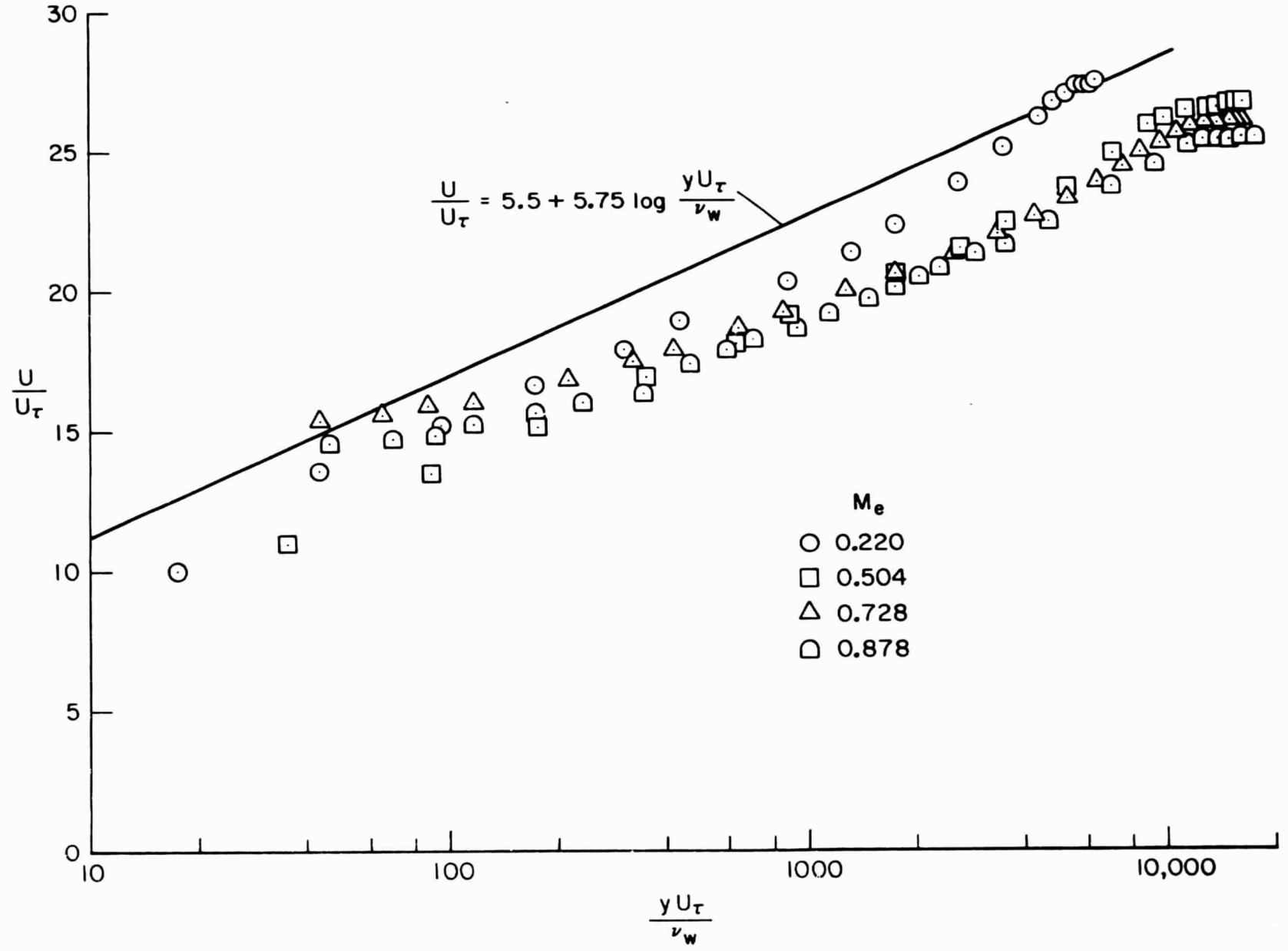

Figure 13.– Velocity profiles in law-of-the-wall coordinates.

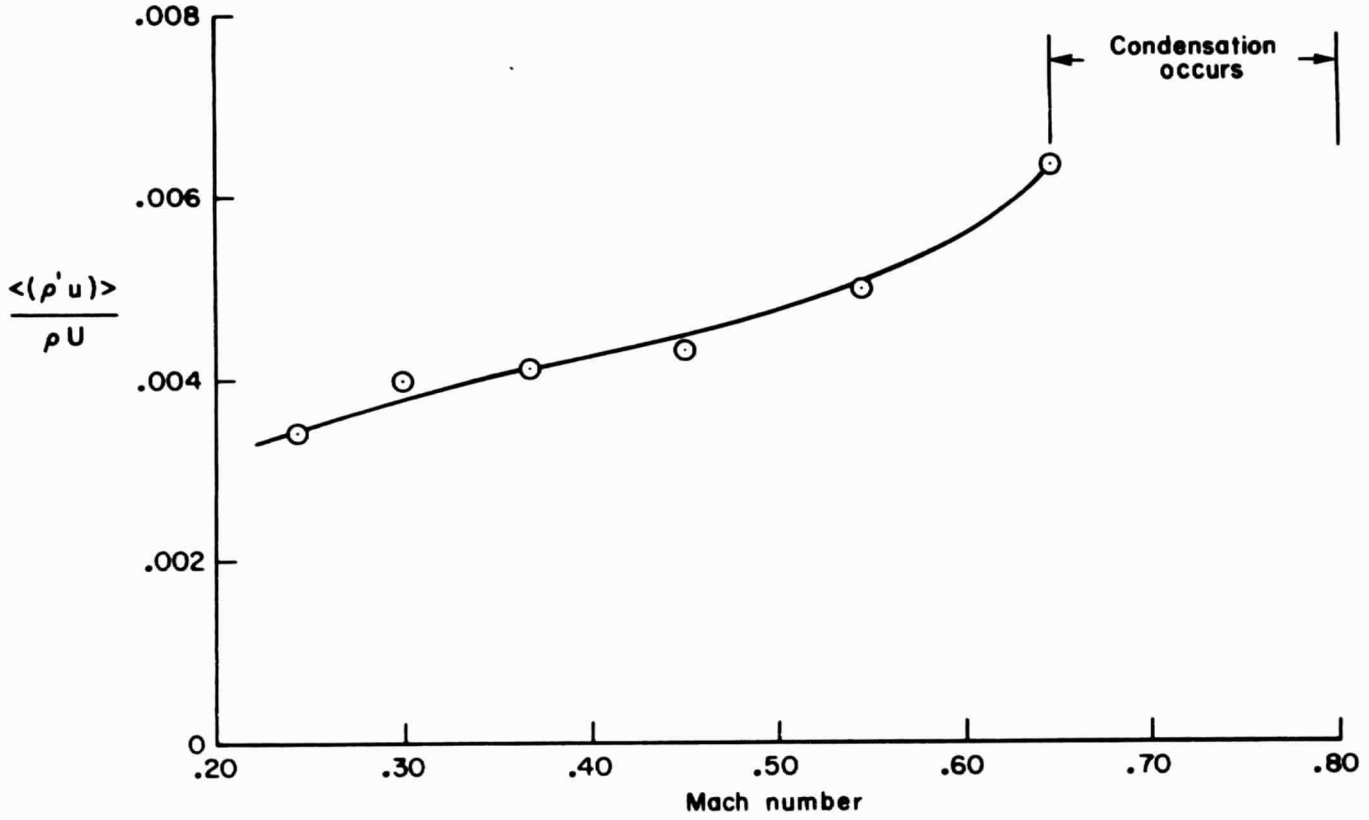

Figure 14.– Turbulent intensity along the channel centerline.

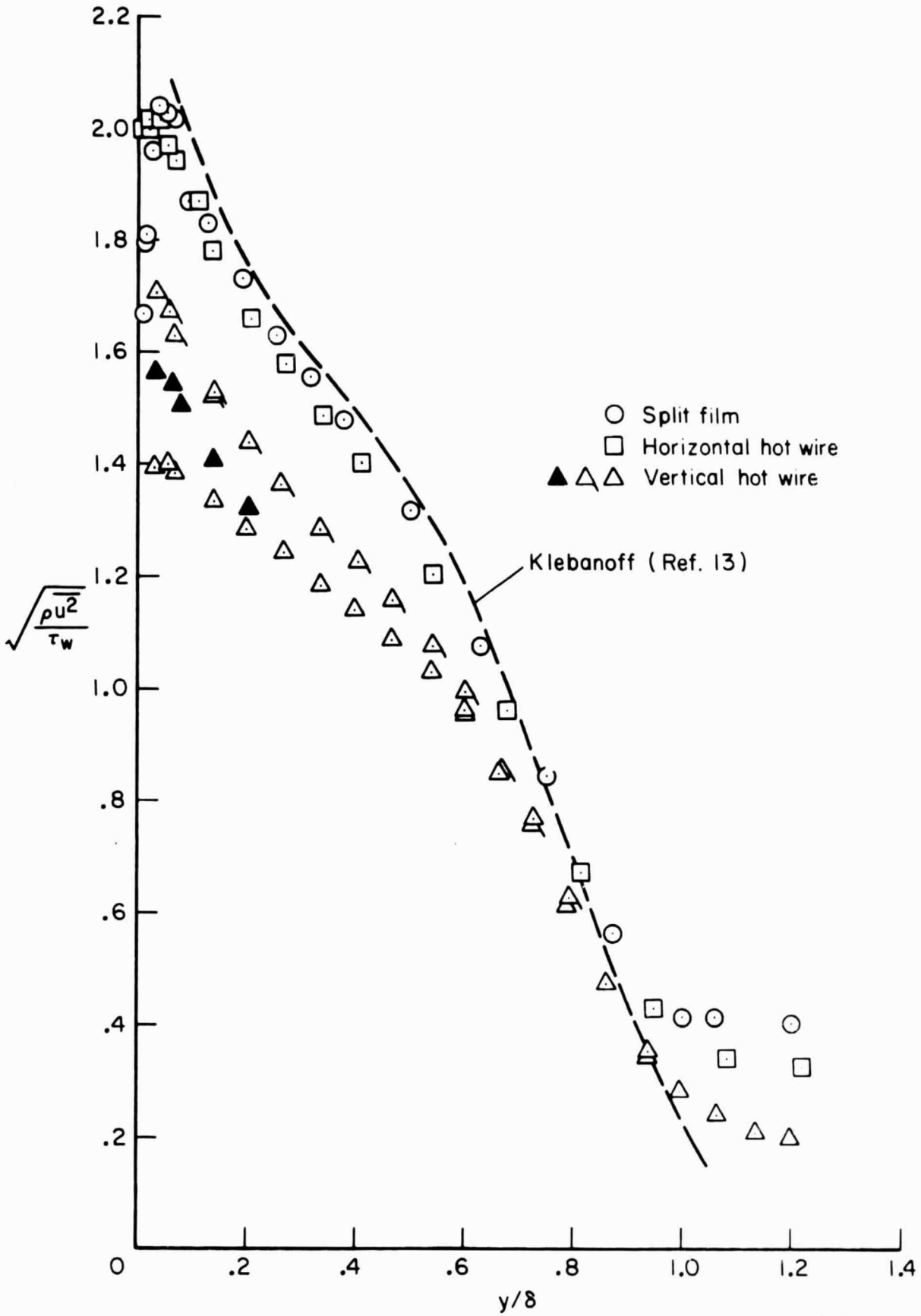

Figure 15.– Comparison of the split-film measurements of the longitudinal turbulent velocity with a hot wire at $M_e \approx 0.22$.

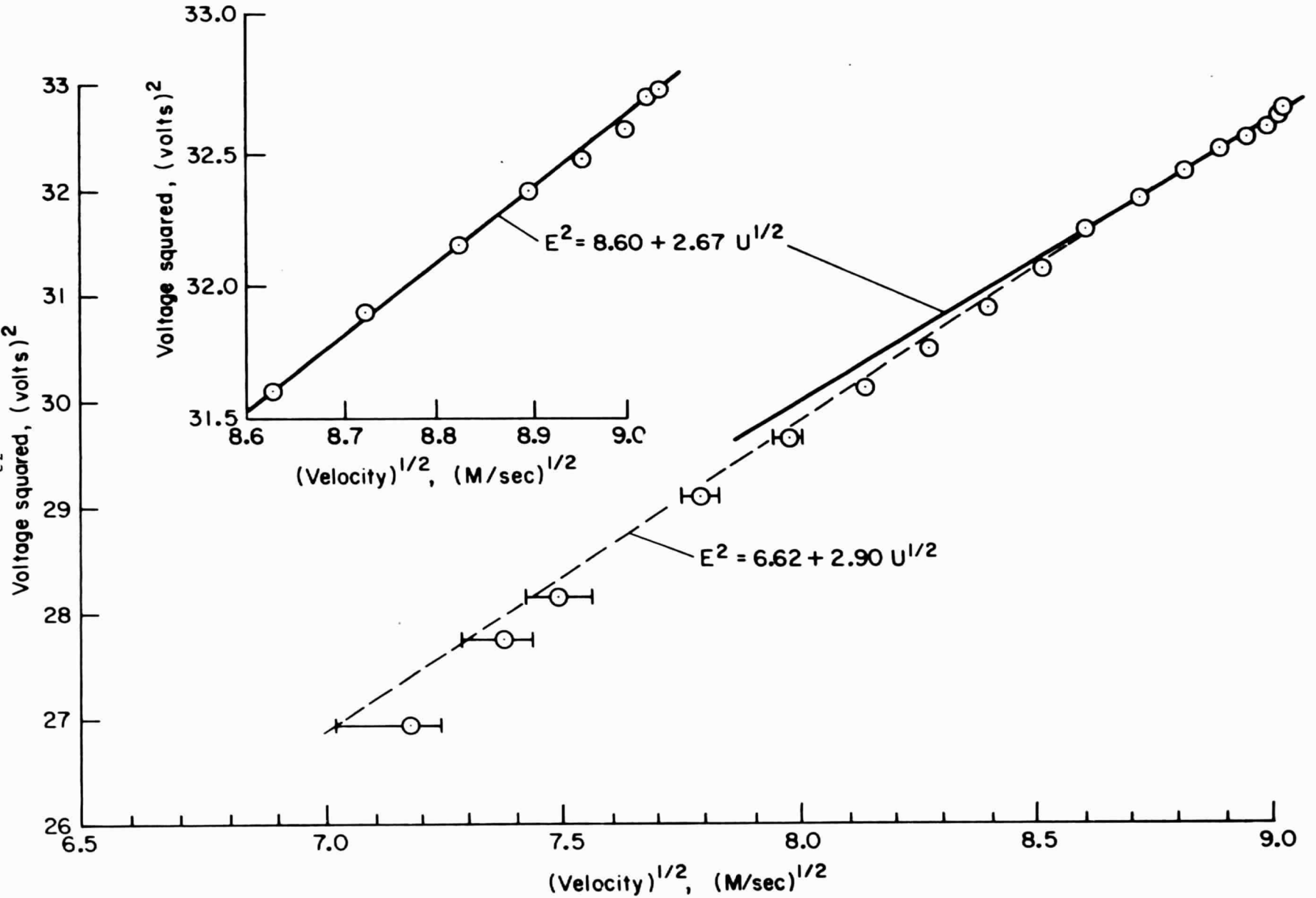

Figure 16.– King's Law plot of the vertical hot-wire output.

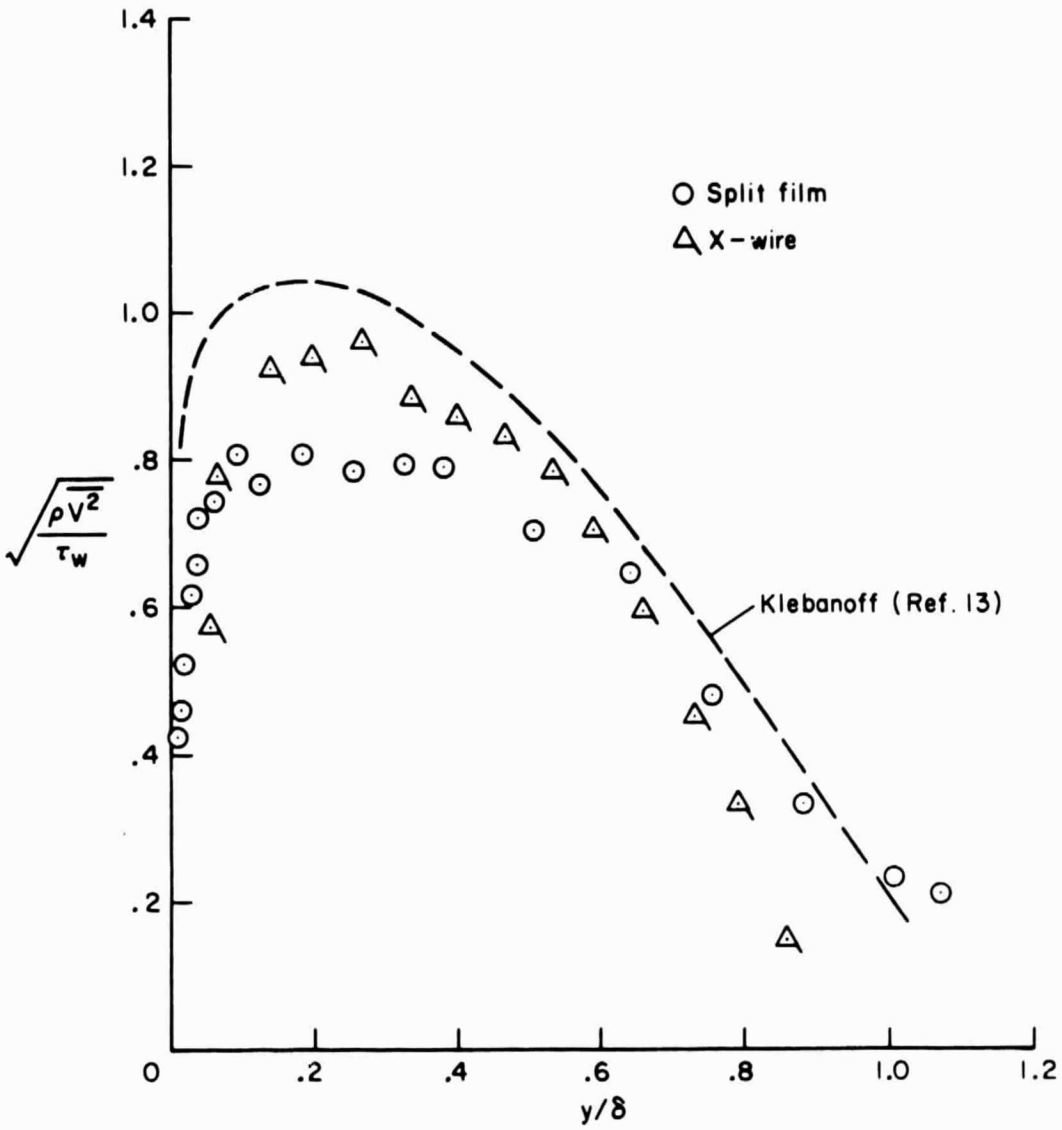

Figure 17.– Comparison of the split-film measurements of the vertical turbulent velocity with an X-wire at $M_e \approx 0.22$.

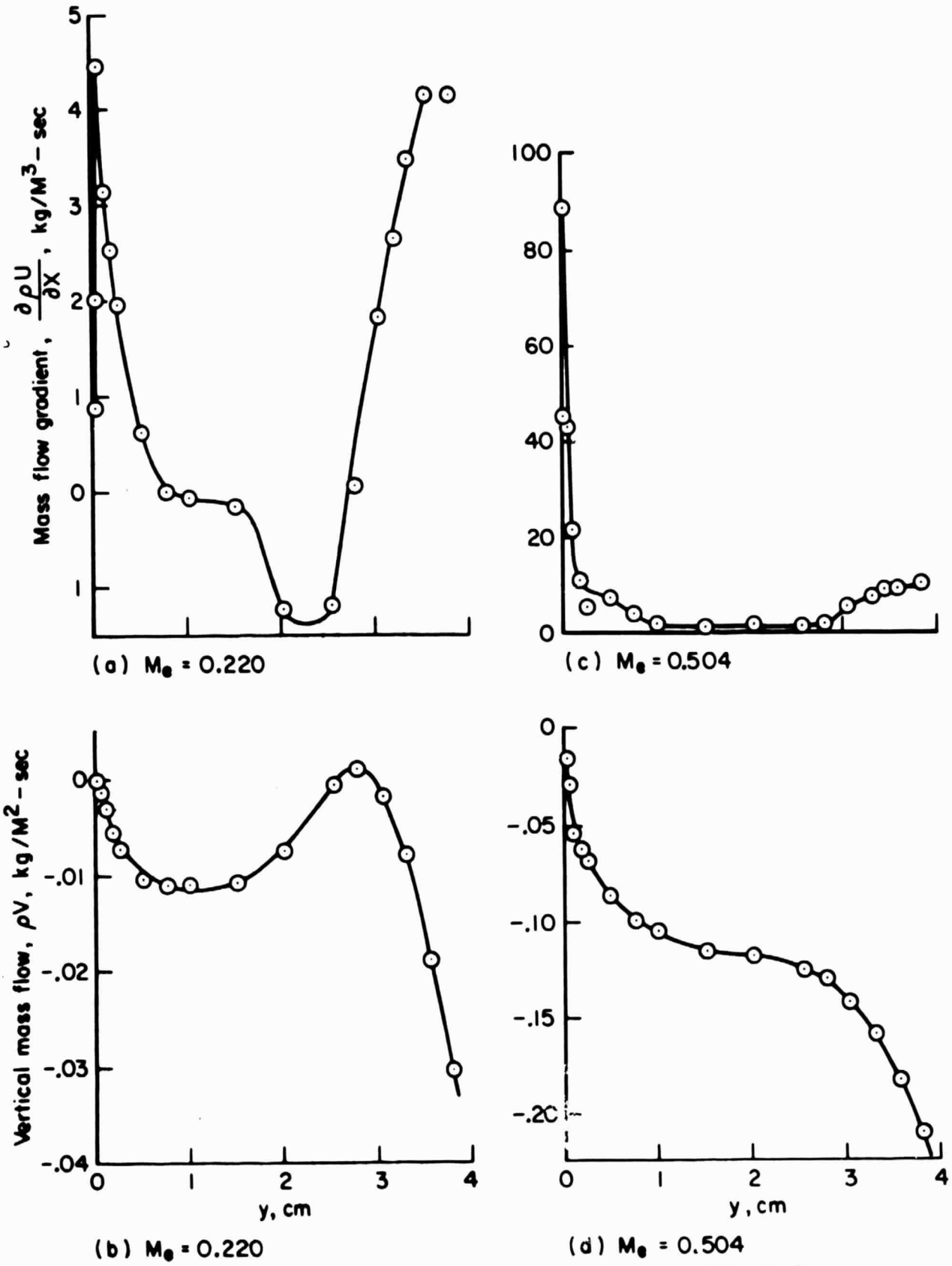

Figure 18.– Variation of the mass flow gradient and the vertical mass flow across the boundary layer.

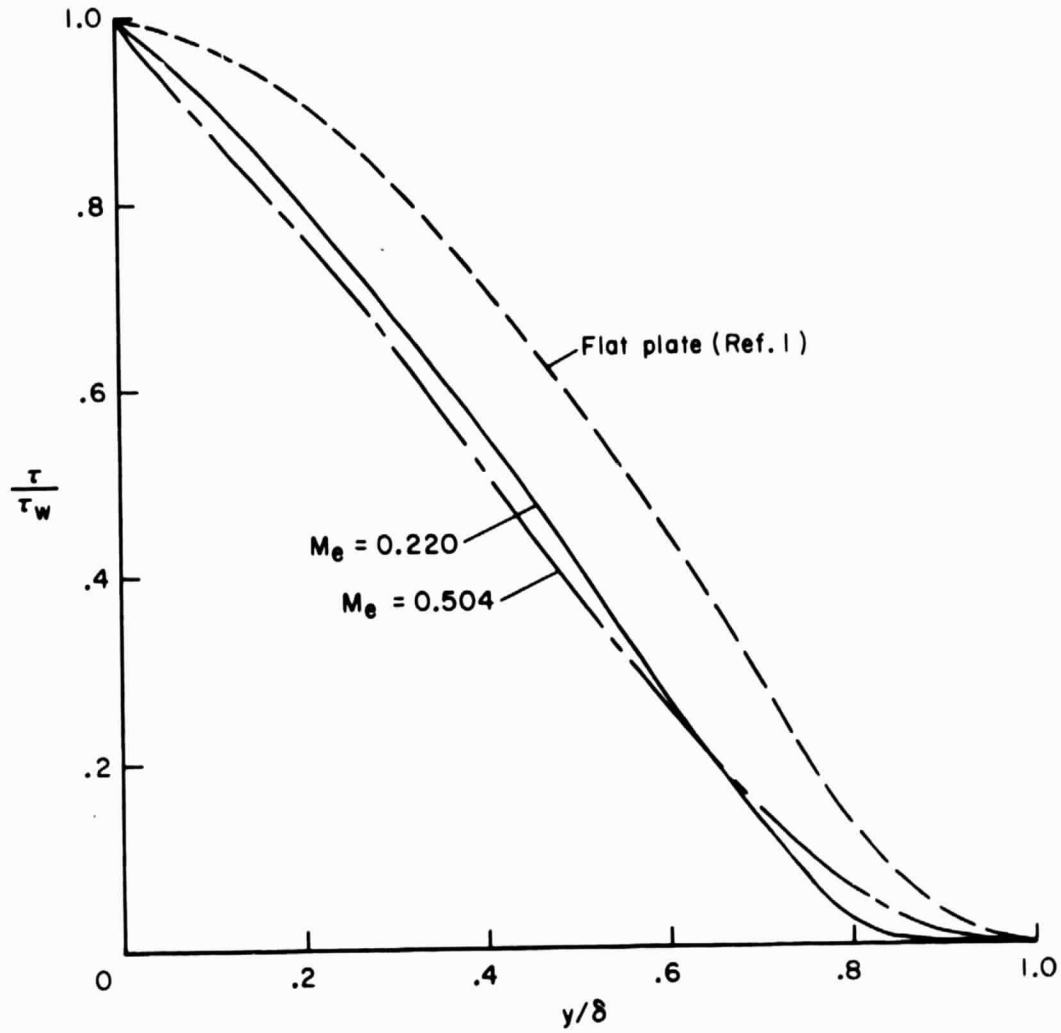

Figure 19.– Evaluation of the total shear-stress distribution.

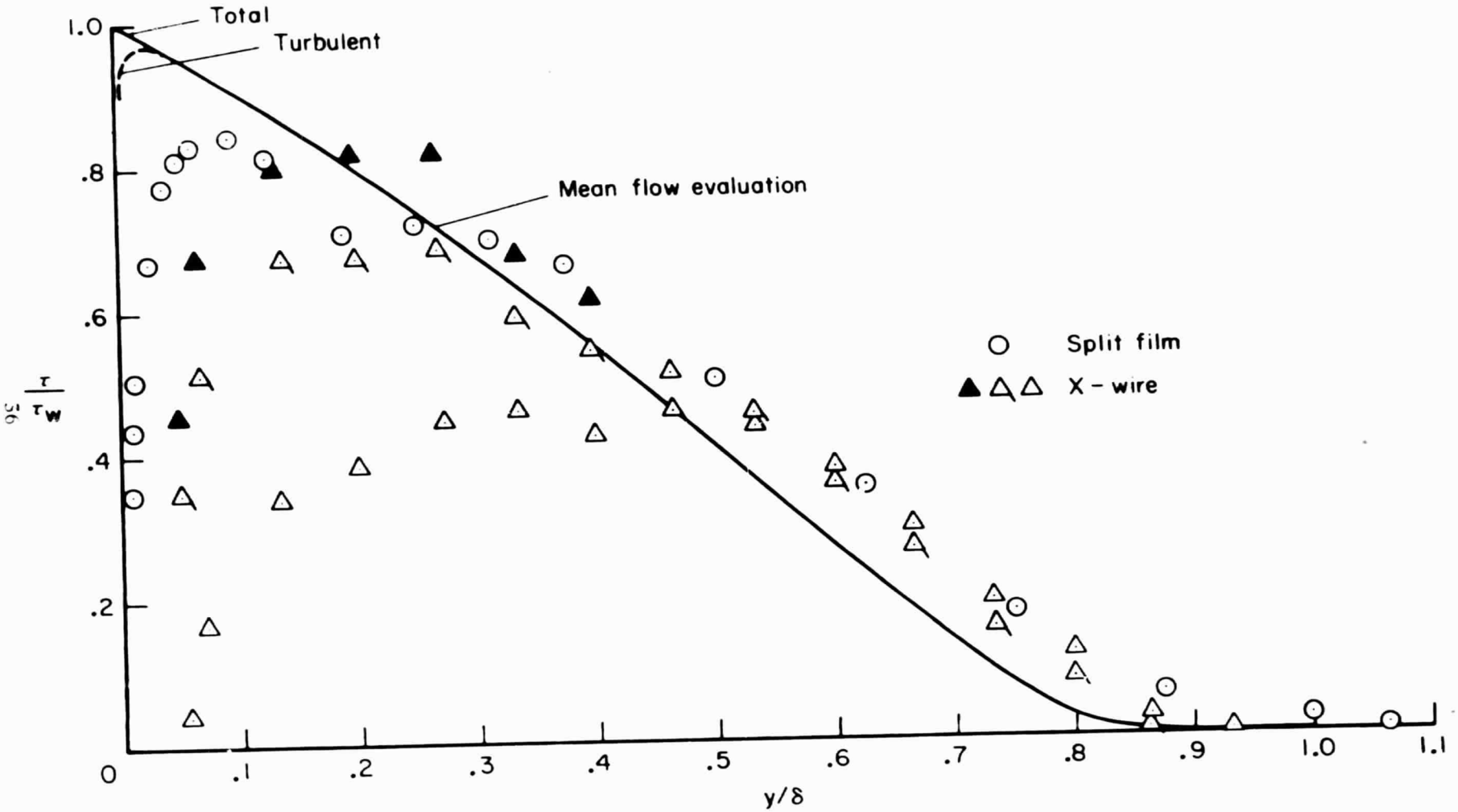

Figure 20.– Comparison of the split-film measurements of turbulent shear stress with an X-wire at $M_e \approx 0.22$.

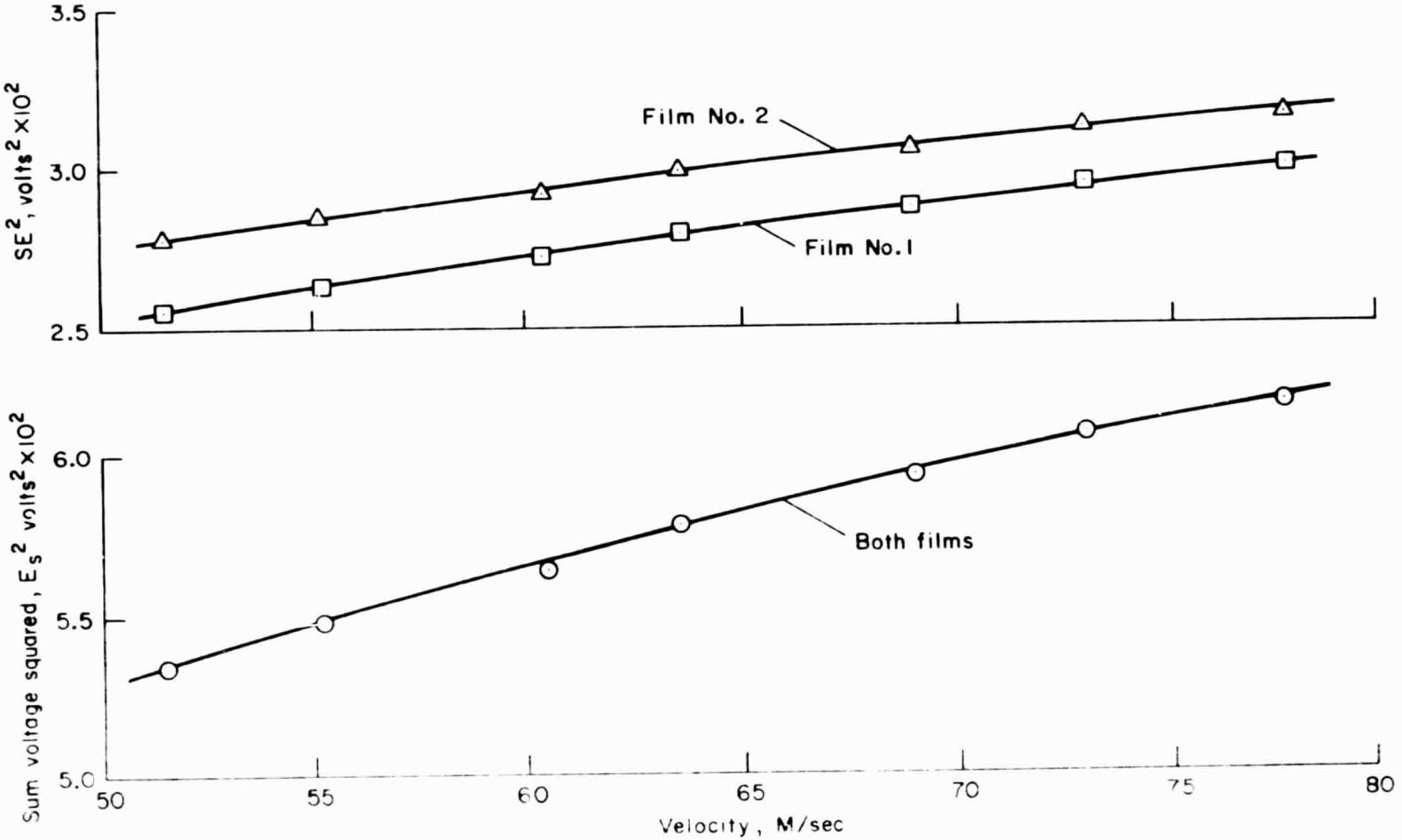

Figure 21. Typical voltage-velocity calibration of a split-film sensor.

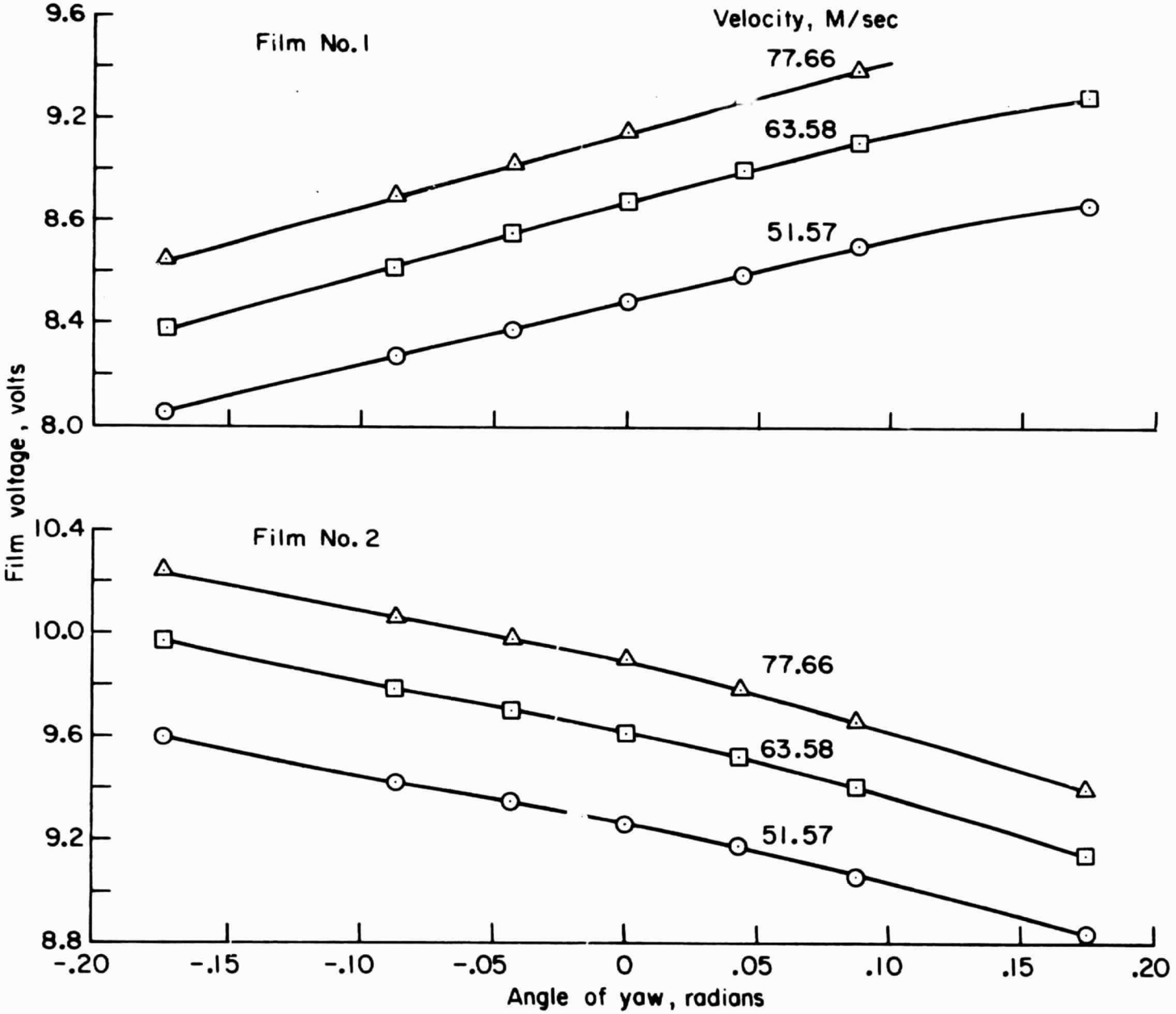

Figure 22.– Evaluation of the angle sensitivity of the split-film sensor.

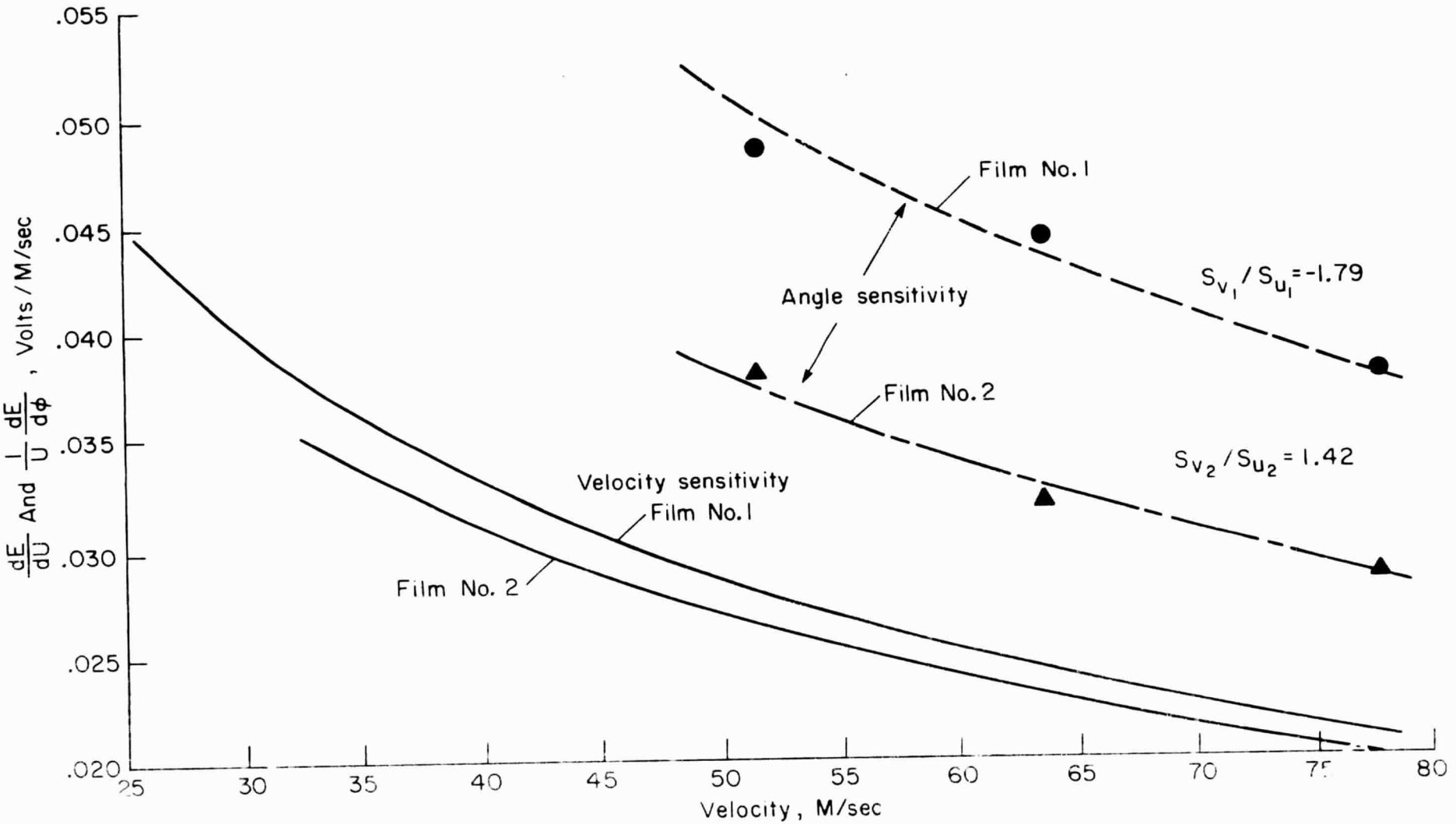

Figure 23. Velocity and angle sensitivities of the splat-film sensor.